MABS
2025, VOL. 17, NO. 1, 2498164
https://doi.org/10.1080/19420862.2025.2498164

Taylor & Francis
Taylor & Francis Group

REPORT



# Development of potent humanized TNFα inhibitory nanobodies for therapeutic applications in TNFα-mediated diseases

Tao Yin[a], Aubin Ramon[b], Matthew Greenig[b], Pietro Sormanni[b], and Luciano D'Adamio[a,c]

[a]Department of Pharmacology, Physiology & Neuroscience New Jersey Medical School, Brain Health Institute, Jacqueline Krieger Klein Center in Alzheimer's Disease and Neurodegeneration Research, Rutgers, The State University of New Jersey, Newark, NJ, USA; [b]Centre for Misfolding Diseases, Yusuf Hamied Department of Chemistry, University of Cambridge, Cambridge, UK; [c]Founder of NanoNewron LLC, Union, NJ, USA

**ABSTRACT**

Tumor necrosis factor-alpha (TNFα) is a key pro-inflammatory cytokine implicated in the pathogenesis of numerous inflammatory and autoimmune diseases, including rheumatoid arthritis, inflammatory bowel disease, and neurodegenerative disorders such as Alzheimer's disease. Effective inhibition of TNFα is essential for mitigating disease progression and improving patient outcomes. In this study, we present the development and comprehensive characterization of potent humanized TNFα inhibitory nanobodies (TNFI-Nbs) derived from camelid single-domain antibodies. In silico analysis of the original camelid nanobodies revealed low immunogenicity, which was further reduced through machine learning-guided humanization and developability optimization. The two humanized TNFI-Nb variants we developed demonstrated high anti-TNFα activity, achieving $IC_{50}$ values in the picomolar range. Binding assays confirmed their high affinity for TNFα, underscoring robust neutralization capabilities. These TNFI-Nbs present valid alternatives to conventional monoclonal antibodies currently used in human therapy, offering potential advantages in potency, specificity, and reduced immunogenicity. Our findings establish a solid foundation for further preclinical development and clinical translation of TNFα-targeted nanobody therapies in TNFα-mediated diseases.

**ARTICLE HISTORY**
Received 11 February 2025
Revised 21 April 2025
Accepted 22 April 2025

**KEYWORDS**
Alzheimer disease; nanobody; single-domain antibody; TNFα; TNFα inhibition; nanobody humanization

## Introduction

The pathogenesis of numerous inflammatory and autoimmune diseases is linked to the pro-inflammatory cytokine tumor necrosis factor-alpha (TNFα). Biologic TNFα inhibitors (TNFI), including conventional monoclonal antibodies, have revolutionized the treatment of peripheral TNFα-mediated conditions,[1–5] but conventional antibodies have limitations such as large molecular size, potential immunogenicity, and restricted tissue penetration.

Nanobodies, which are single-domain antibodies derived from camelid species, offer a promising alternative to conventional antibodies.[6,7] These molecules consist of a single monomeric variable antibody domain, featuring smaller paratopes that can access functional pockets of target proteins more efficiently. This results in enhanced binding specificity, affinity, and inhibitory efficiency, allowing nanobodies to recognize and bind epitopes often inaccessible to traditional antibodies, thereby broadening therapeutic targets. Additionally, their smaller size (~12 kDa compared to ~150 kDa for conventional antibodies) reduces the potential for immunogenicity and facilitates better tissue penetration. Nanobodies also exhibit exceptional stability under a wide range of physiological conditions, including extreme pH and temperature, which is advantageous for storage, formulation, and administration. Unlike conventional anti-TNFα biologics such as adalimumab (Humira), which contain an Fc domain that can mediate antibody-dependent cellular cytotoxicity (ADCC) and complement-dependent cytotoxicity (CDC), nanobodies lack an Fc region. This eliminates the risk of Fc-mediated immune activation, reducing the likelihood of immune-related adverse effects and making them better suited for chronic administration in autoimmune diseases. By minimizing systemic immunosuppression while maintaining potent TNFα neutralization, nanobodies provide a safe and targeted therapeutic approach. Additionally, nanobody-based TNFI offer substantial advantages in manufacturing and cost-effectiveness. Their simpler structure allows for efficient production, thereby reducing production costs. This makes nanobody-based therapeutics a scalable and accessible option for treating TNFα-driven diseases. However, further improvements are necessary to maximize their utility in peripheral inflammatory therapies, ensuring sustained therapeutic action and minimizing the need for frequent dosing. Nevertheless, the fact that ozoralizumab (Nanozora®), an anti-TNFα nanobody-based biologic, is approved and marketed in Japan for rheumatoid arthritis supports the potential of this approach for clinical application in humans.

Beyond peripheral inflammatory conditions, nanobodies hold potential for the treatment of central nervous system (CNS) diseases. Conventional antibodies have limited blood–

**CONTACT** Luciano D'Adamio luciano.dadamio@rutgers.edu Department of Pharmacology, Physiology & Neuroscience New Jersey Medical School, Brain Health Institute, Jacqueline Krieger Klein Center in Alzheimer's Disease and Neurodegeneration Research, Rutgers, The State University of New Jersey, 205 South Orange Avenue, Newark, NJ 0703, USA

Supplemental data for this article can be accessed online at https://doi.org/10.1080/19420862.2025.2498164

brain barrier (BBB) permeability, restricting their effectiveness in targeting CNS pathologies. In contrast, the smaller size and robust structural stability of nanobodies may facilitate better BBB penetration,[8,9] enhancing their therapeutic reach within the brain. Moreover, their inherent ability to be engineered for improved BBB permeability opens avenues for innovative delivery strategies, such as receptor-mediated transcytosis via transferrin receptor 1 (TfR1),[10–13] potentially increasing their efficacy in treating neurodegenerative disorders.

In this study, we present the development and characterization of potent humanized TNFα inhibitory nanobodies (TNFI-Nbs) derived from camelid single-domain antibodies. By leveraging advances in in-silico analysis and machine-learning-guided mutagenesis, we optimized the framework of TNFI-Nbs to maximize humanness and solubility while retaining and slightly improving affinity for TNFα.

## Results

### Generation of anti-human TNFα nanobodies

To generate nanobodies specifically targeting human TNFα, one llama and one alpaca were immunized with active trimeric human TNFα (Acro Biosystems, TNA-H5228) to elicit a robust immune response. Serum titers from the immunized animals were monitored and quantified using ELISA on antigen-coated plates to confirm the production of high-affinity antibodies. Peripheral blood mononuclear cells (PBMCs) were isolated and cDNAs encoding the VHH domains of nanobodies were cloned into the pADL-20c phagemid vector and transformed into *E. coli* TG cells for phage display.

To enrich nanobody clones with strong binding to human TNFα, multiple rounds of panning were performed on antigen-coated plates, a process designed to selectively capture high-affinity clones while removing nonspecific or weak binders. After enrichment, 470 individual nanobody clones were expressed in *E. coli*, and His-tagged nanobodies were recovered from the periplasmic fraction via osmotic shock. These nanobodies were screened for their ability to bind human TNFα by ELISA, leading to the identification of α-TNFα nanobodies (α-TNFα-Nbs) with strong antigen interaction. The term α-TNFα-Nbs simply denotes nanobodies that bind to TNFα, whereas TNFI-Nbs specifically refer to nanobodies that not only bind to TNFα but also inhibit its cytotoxic activity. Sequencing of ELISA-positive clones revealed 100 unique α-TNFα-Nb sequences, each representing a distinct nanobody (Figure 1). These 100 unique nanobodies were then expressed in bacterial cultures and purified using affinity chromatography. The purified α-TNFα-Nbs underwent further functional characterization.

The above experiments were performed at Abcore, a contract research organization specializing in the generation of custom antibodies, including nanobodies, for research and therapeutic applications. A detailed summary of Abcore's experimental procedures is provided in the Supporting information data file entitled: *Identification, Cloning, and Production of α-TNFα-Nbs.*

### Identification of α-TNFα nanobodies with high inhibitory activity against human TNFα (TNFI-Nbs)

The 100 purified α-TNFα-Nbs were assessed for their ability to inhibit cytotoxicity induced by active trimeric human TNFα. Initial screening utilized WEHI-13VAR cells, a mouse line that serves as a sensitive bioassay for both rodent and human TNFα. WEHI-13VAR cells were incubated for 24 hours with 0.25 ng/mL active trimeric human TNFα and 1 μg/mL Actinomycin-D, either alone or in the presence of 100 nM of each α-TNFα-Nb. Cytotoxicity was measured using the Cell Counting Kit-8, comparing cell viability to that of cells treated with Actinomycin-D alone. Eleven α-TNFα-Nbs that achieved at least 60% inhibition of human TNFα–induced cell death at 100 nM concentration (data not shown) were selected for further evaluation. In the secondary screening, these selected α-TNFα-Nbs underwent twofold serial dilutions ranging from 100 nM to 0.76294 pM. Secondary screening identified three nanobodies (05C08R3, 05B05R3, and 03H04R3) with strong TNFα inhibitory activity, exhibiting $IC_{50}$ values of 95.78 pM (95% confidence interval [CI]: 78.24–116.4 pM), 219.3 pM (95% CI: 178.7–268.3 pM), and 175 pM (95% CI: 136–222.7 pM), respectively (Figure 2a). Consequently, these α-TNFα nanobodies were renamed TNFI-Nb1, TNFI-Nb2, and TNFI-Nb3.

To analyze the sequence and structural features of the three selected nanobodies, we adopted the AHo numbering system instead of other commonly used schemes such as IMGT, Kabat, and Chothia. While these systems are generally comparable, AHo offers a key advantage by being structure-based: it introduces alignment gaps at the structural tips of the complementarity-determining region (CDR) loops, making it more representative of the actual antigen-binding interface and functional conformation. In contrast, IMGT is primarily based on germline gene recombination boundaries, which may not align with the final folded structure or binding properties of the nanobody.

Our analysis revealed that the three nanobodies share identical CDRs, with all sequence differences restricted to framework regions 1 and 3 (Table 1). This strongly suggests that they belong to the same nanobody family, and their identical CDRs likely explain their similarly high TNFα inhibitory activity. Supporting this conclusion, these three nanobodies were the only members of this family identified among the 100 unique clones analyzed (Figure 1). Consistently, each nanobody aligns with the same closest human and alpaca V-genes and exhibits comparable percent sequence identity, further confirming a shared germline origin.

To further characterize the specificity of TNFI-Nb1, TNFI-Nb2, and TNFI-Nb3, we evaluated their ability to inhibit cytotoxicity induced by rat and mouse TNFα. Using the same assay conditions described for human TNFα inhibition, WEHI-13VAR cells were incubated for 24 hours with active trimeric rat TNFα or mouse TNFα in the presence of each nanobody. The nanobodies were tested at a concentration of 100 nM, followed by twofold serial dilutions ranging from 100 nM to 0.76294 pM (Figure 2b). None of the three TNFI-Nbs were able to inhibit cytotoxicity induced by either rat or mouse TNFα at any of the concentrations tested. This lack of inhibitory activity underscores the high specificity of these

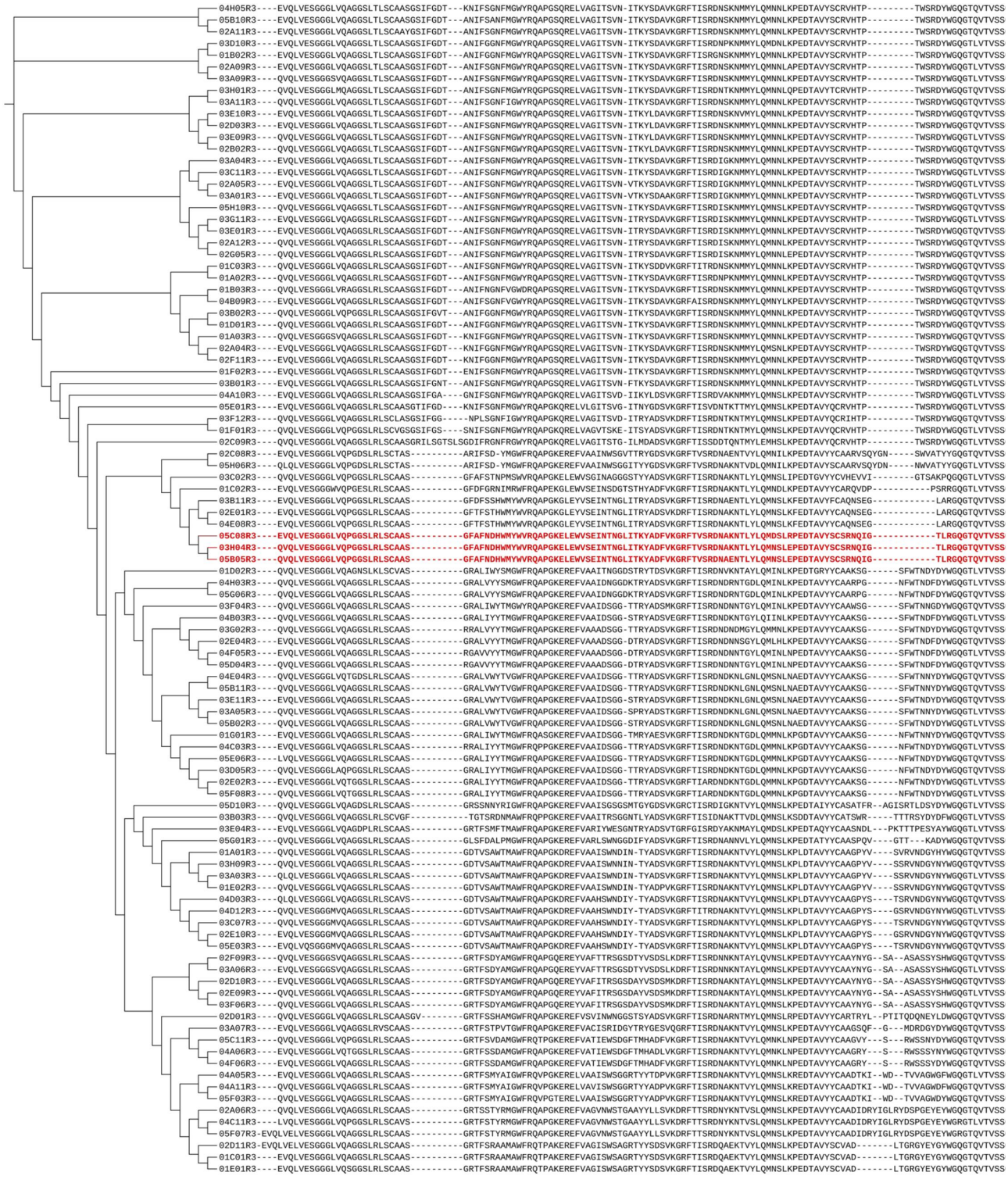

**Figure 1.** Phylogenetic analysis and amino acid sequences of 100 unique α-TNFα nanobodies (nbs) isolated from immunized alpaca and Llama.

nanobodies for human TNFα. This selectivity for human TNFα makes standard rodent models unsuitable for evaluating the biological activities of TNFI-Nb1, TNFI-Nb2, and TNFI-Nb3. Therefore, humanized animal models or in vitro systems expressing human TNFα are necessary to investigate their therapeutic potential and mechanisms of action. These models will enable accurate assessment of the nanobodies' efficacy and safety, providing essential data for advancing to clinical trials.

Finally, we evaluated whether TNFI-Nb1, TNFI-Nb2, and TNFI-Nb3 can bind to membrane-bound TNFα. To achieve this, HEK293 cells were transfected with a construct expressing human TNFα and enhanced green fluorescent protein (EGFP) to label the transfected cells. As shown in Figure 2c, flow cytometry (FACS) analysis revealed that all three TNFI-Nbs bound to the transfected cells, demonstrating their ability to recognize and interact with membrane-bound TNFα.

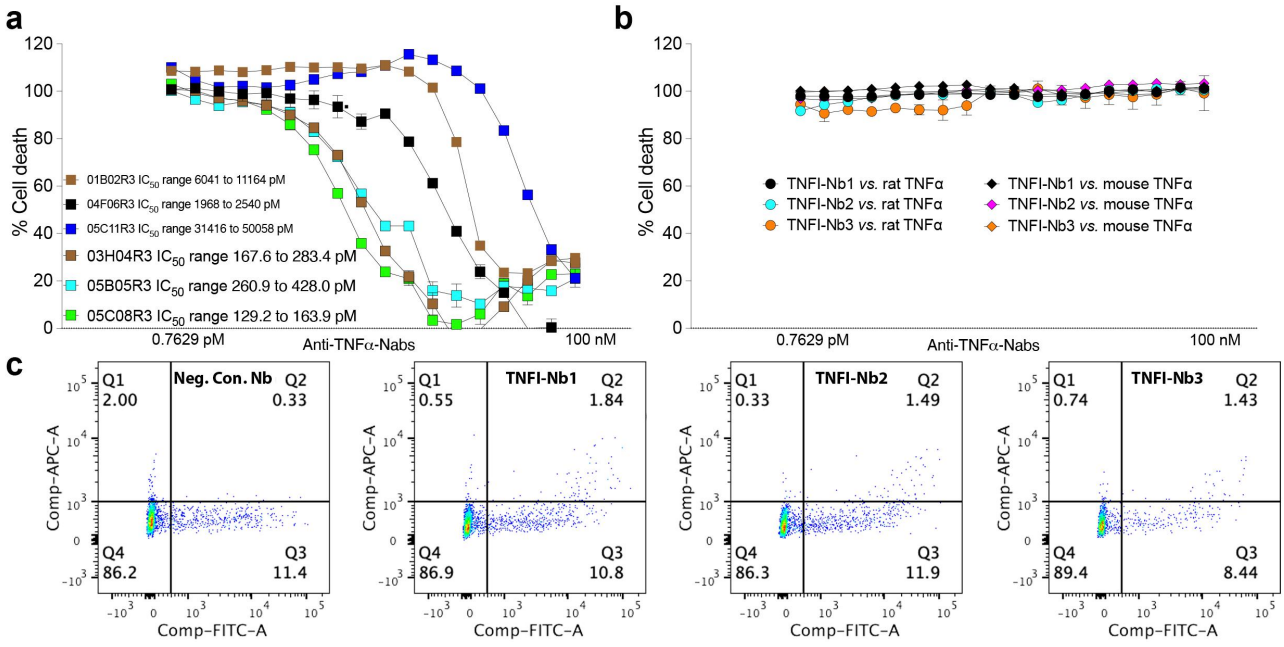


**Figure 2.** TNFI-Nb1, TNFI-Nb2, and TNFI-Nb3 exhibit potent, human-specific TNFα inhibition and bind membrane-bound TNFα.

### *Production of TNFI-Nbs in CHO-S cells*

Chinese hamster ovary (CHO) cells are a preferred system to produce therapeutic proteins due to their ability to generate complex proteins with proper folding, post-translational modifications, and biological activity like native human proteins. Another advantage of using CHO cells is their ability to produce proteins with significantly lower endotoxin levels compared to bacterial expression systems, enhancing the safety and suitability of the final product for therapeutic use. Therefore, this system minimizes the risk of immunogenicity by ensuring the produced proteins are more likely to be recognized as "self" by mammalian immune systems. Given their long history of regulatory approval for numerous therapeutic proteins, CHO cells provide a reliable platform for biopharmaceutical manufacturing.

To determine the optimal production system for TNFI-Nb1, we compared protein production efficiency and quality between *E. coli* and CHO-S cells. CHO-S cells produced 16.52 mg of TNFI-Nb1 from a 100 mL culture at a concentration of 1.18 mg/mL, with a purity of ≥ 95% as assessed by SDS-PAGE and 96% by SEC-HPLC. Endotoxin levels in the CHO-S-derived protein were ≤ 0.1 EU/mg, well below acceptable thresholds for therapeutic use. It is important to note that these substantial, yet not exceptional, production levels were achieved through transient transfection without selecting high-producing stable clones or implementing further process optimization. In contrast, *E. coli* yielded only 2.1 mg of TNFI-Nb1 from a 1 L culture at a concentration of 0.35 mg/mL, with lower purity (≥90% by SDS-PAGE) and significantly higher endotoxin levels (≤10.9 EU/mg). These results clearly demonstrate the superiority of CHO-S cells in terms of yield, purity, and endotoxin levels.

Based on these findings, we produced TNFI-Nb2 and TNFI-Nb3 in 100 mL CHO-S cell cultures. TNFI-Nb2 was obtained at a yield of 14.26 mg (0.92 mg/mL) with a purity of ≥ 90% as assessed by SDS-PAGE and 94% by SEC-HPLC, and endotoxin levels ≤ 0.1 EU/mg. TNFI-Nb3 was produced at 13.64 mg (0.88 mg/mL) with a purity of ≥ 95% by SDS-PAGE and 95% by SEC-HPLC, and endotoxin levels ≤ 0.1 EU/mg. Protein production was performed at GenScript, and detailed experimental procedures and results are provided in the Supporting information data file entitled: *TNFI-Nb Production in CHO-S cells*.

### *Surface plasmon resonance analysis of TNFI-Nb1-3 binding to human TNFα*

To determine the binding affinity of TNFI-Nb1, TNFI-Nb2, and TNFI-Nb3 to human TNFα, we conducted surface plasmon resonance (SPR) analysis. The purity of all three nanobodies, TNFI-Nb1 (05C08R3,VHH1), TNFI-Nb2 (05B05R3, VHH2), and TNFI-Nb3 (03H04R3, VHH3), as well as human TNFα, was confirmed to exceed 90%, ensuring high-quality reagents for subsequent assays. Kinetic analyses were performed using Cytiva's Biacore 1K SPR system and Nicoya's OpenSPR-XT instrument with Carboxyl CM5 sensors. Assay optimization encompassed the screening of various immobilization conditions, buffer formulations, and regeneration protocols to establish a reliable and reproducible measurement framework. Optimal immobilization was achieved using the nanobodies and the ligands at a concentration of 2.5 μg/mL in 10 mm acetate buffer (pH 4.5), resulting in appropriate response maxima (Rmax) for each nanobody and ensuring sufficient signal for accurate kinetic fitting. Buffer optimization identified 1× phosphate-buffered saline (PBS) supplemented with 3 mM EDTA and 0.05% v/v Surfactant P20 as the optimal running buffer, effectively minimizing nonspecific binding and maximizing signal-to-noise ratios.

Multi-cycle kinetic analysis revealed that all three nanobodies interacted with TNFα following a 1:1 binding model,

**Table 1.** Alignment and V-gene identities of the sequences of TNFI-Nb1, 2, and 3.

| **Aho number:** | 1 | 2 | 3 | 4 | 5 | 6 | 7 | 9 | 10 | 11 | 12 | 13 | 14 | 15 | 16 | 17 | 18 | 19 | 20 | 21 | 22 | 23 | 24 |
|---|---|---|---|---|---|---|---|---|---|---|---|---|---|---|---|---|---|---|---|---|---|---|---|
| **TNFI-Nb1** | E | V | Q | L | V | E | S | G | G | G | L | V | Q | P | G | G | S | L | R | L | S | C | A |
| **TNFI-Nb2** | **Q** | V | Q | L | V | E | S | G | G | G | L | V | Q | P | G | G | S | L | R | L | S | C | A |
| **TNFI-Nb3** | **Q** | V | Q | L | V | E | S | G | G | G | L | V | Q | P | G | G | S | L | R | L | S | C | A |
| **Aho number:** | 25 | 26 | 27 | 28 | 29 | 30 | 31 | 38 | 39 | 40 | 41 | 42 | 43 | 44 | 45 | 46 | 47 | 48 | 49 | 50 | 51 | 52 | 53 |
| **TNFI-Nb1** | A | S | G | F | A | F | N | D | H | W | M | Y | W | V | R | Q | A | P | G | K | E | L | E |
| **TNFI-Nb2** | A | S | G | F | A | F | N | D | H | W | M | Y | W | V | R | Q | A | P | G | K | E | L | E |
| **TNFI-Nb3** | A | S | G | F | A | F | N | D | H | W | M | Y | W | V | R | Q | A | P | G | K | E | L | E |
| **Aho number:** | 54 | 55 | 56 | 57 | 58 | 59 | 60 | 61 | 65 | 66 | 67 | 68 | 69 | 70 | 71 | 72 | 73 | 74 | 75 | 76 | 77 | 78 | 79 |
| **TNFI-Nb1** | W | V | S | E | I | N | T | N | G | L | I | T | K | Y | A | D | F | V | K | G | R | F | T |
| **TNFI-Nb2** | W | V | S | E | I | N | T | N | G | L | I | T | K | Y | A | D | F | V | K | G | R | F | T |
| **TNFI-Nb3** | W | V | S | E | I | N | T | N | G | L | I | T | K | Y | A | D | F | V | K | G | R | F | T |
| **Aho number:** | 80 | 81 | 82 | 83 | 84 | 85 | 86 | 87 | 88 | 89 | 90 | 91 | 92 | 93 | 94 | 95 | 96 | 97 | 98 | 99 | 100 | 101 | 102 |
| **TNFI-Nb1** | V | S | R | D | N | A | K | N | T | L | Y | L | Q | M | D | S | L | R | P | E | D | T | A |
| **TNFI-Nb2** | V | S | R | D | N | A | K | N | T | L | Y | L | Q | M | **N** | S | L | **E** | P | E | D | T | A |
| **TNFI-Nb3** | V | S | R | D | N | A | **E** | N | T | L | Y | L | Q | M | **N** | S | L | **E** | P | E | D | T | A |
| **Aho number:** | 103 | 104 | 105 | 106 | 107 | 108 | 109 | 110 | 111 | 136 | 137 | 138 | 139 | 140 | 141 | 142 | 143 | 144 | 145 | 146 | 147 | 148 | 149 |
| **TNFI-Nb1** | V | Y | S | C | S | R | N | Q | I | G | T | L | R | G | Q | G | T | Q | V | T | V | S | S |
| **TNFI-Nb2** | V | Y | S | C | S | R | N | Q | I | G | T | L | R | G | Q | G | T | Q | V | T | V | S | S |
| **TNFI-Nb3** | V | Y | S | C | S | R | N | Q | I | G | T | L | R | G | Q | G | T | Q | V | T | V | S | S |

| | **Closest human V-gene** | **Identity to closest human V-gene (%)** | **Closest alpaca V-gene** | **Identity to closest alpaca V-gene (%)** |
|---|---|---|---|---|
| **TNFI-Nb1** | IGHV3-74*01 | 0.81 | IGHV3S1*01 | 0.81 |
| **TNFI-Nb2** | IGHV3-74*01 | 0.8 | IGHV3S1*01 | 0.83 |
| **TNFI-Nb3** | IGHV3-74*01 | 0.79 | IGHV3S1*01 | 0.82 |

The amino acid sequences of TNFI-Nb1, TNFI-Nb2, and TNFI-Nb3 are aligned using the AHo numbering scheme. All nanobodies share identical CDR1, CDR2, and CDR3 sequences (highlighted in color). Sequence differences, highlighted in bold and gray color, are confined to the framework regions 1 and 3. Below the alignment, the table also reports, for each nanobody sequence, the closest human and alpaca V-genes and the corresponding percent sequence identity.

demonstrating high affinity in the picomolar range (Figure 3a). TNFI-Nb2 exhibited the highest affinity with an equilibrium dissociation constant (KD) of 77 pM, primarily driven by its slower off-rate ($k_d$ ($s^{-1}$) = 2.87E−05 ± 4.6E−06). TNFI-Nb1 displayed a KD of 219 pM, while TNFI-Nb3 showed a KD of 392 pM (Figure 3b). Iso-affinity analysis further confirmed that TNFI-Nb2's superior affinity was mainly due to its slower dissociation rate, distinguishing it from TNFI-Nb1 and TNFI-Nb3 (Figure 3c). These findings collectively highlight the potent TNFα inhibitory capabilities of the nanobody panel, underscoring their potential as effective therapeutic agents. These SPR results confirm the potent and specific binding of TNFI-Nb1, TNFI-Nb2, and TNFI-Nb3 to human TNFα, validating their potential as effective therapeutic agents. SPR experiments were performed at Rapid Novor.

## *In-silico immunogenicity prediction of TNFI-Nb1, TNFI-Nb2, and TNFI-Nb3*

To evaluate the immunogenicity risk of TNFI-Nabs, we used the iTope-AI platform in conjunction with the TCED™ database. iTope-AI is an in-silico immunogenicity risk assessment and deimmunization tool powered by augmented intelligence, utilizing a state-of-the-art machine learning algorithm to predict peptide binding to HLA class II isotypes DR, DP, and DQ. The platform includes 46 common HLA alleles worldwide, ensuring broad population coverage without bias toward any specific ethnic group. Key binding residues were identified through the generation of overlapping 9-mer peptides, each overlapping by eight amino acids, spanning the entire protein sequence. In-house evaluation by Abzena confirmed that iTope-AI accurately predicts 95% of peptide binding core motifs identified by X-ray crystallography and correctly predicts known promiscuous HLA binders, demonstrating high specificity.

iTope-AI assigns binding scores (0–3) to each peptide for each HLA class II allotype, summing these to generate a "Position Risk Score" for each peptide. Peptides are categorized as weak (1 and 2) medium (3–5) or strong (6 + ) binders. The "Total Score" for a protein is the sum of all Position Risk Scores, and the highest score ("Hotspot Max") indicates the presence of strong binders or highly promiscuous peptides. Peptides homologous to human proteome sequences are excluded to account for T cell tolerance. Promiscuous binders are cross-referenced with the TCED™ database to identify potential T cell epitopes.

Although high-affinity MHC class II-binding peptides are associated with T cell epitopes,[14,15] predictive models like iTope-AI do not capture all complexities of antigen presentation, including peptide accessibility, MHC binding stability, and T cell repertoire.[16,17] Consequently, iTope-AI tends to overestimate immunogenic potential by considering all possible peptide iterations, though only a subset is processed and recognized in vivo. This inherent discrepancy highlights the conservative nature of in-silico methods, designed to minimize the risk of overlooking potential immunogenic epitopes.

The iTope-AI analysis identified 14 non-germline 9-mer MHC class II-binding peptides for TNFI-Nb1, 13 for TNFI-Nb2, and 13 for TNFI-Nb3, with corresponding risk scores listed in Table 2. Specifically, TNFI-Nb1 achieved a Total Score of 72 and a Hotspot Max of 20, while TNFI-Nb2 and TNFI-Nb3 attained Total Scores of 59 and 62 and Hotspot Max

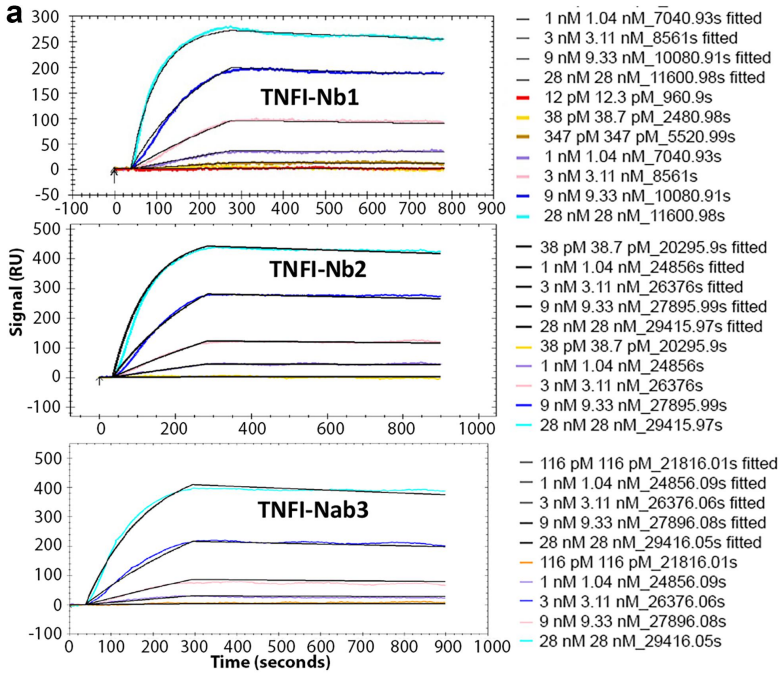


b

| Ligand | Analyte | KD | ka (1/Ms) | kd (1/s) |
|---|---|---|---|---|
| TNFI-Nb1 | TNFα | 219 ± 5.84 pM | 4.89e+05 ± 4.56e+04 | 1.08e-04 ± 1.26e-05 |
| TNFI-Nb2 | TNFα | 77.3 ± 6.28 pM | 3.74e+05 ± 5.93e+04 | 2.87e-05 ± 4.66e-06 |
| TNFI-Nb3 | TNFα | 392.3 ± 65.2 pM | 2.92e+05 ± 3.73e+04 | 1.09e-04 ± 9.14e-06 |

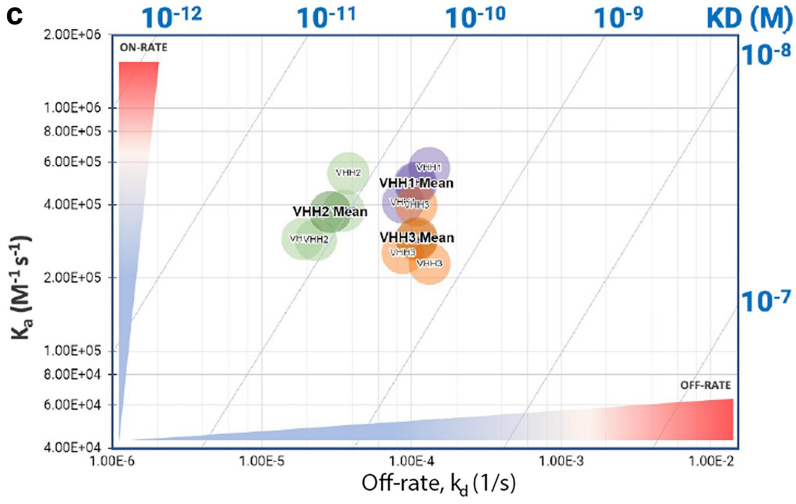


**Figure 3.** Kinetics of TNFα binding to immobilized TNFI-Nb1, TNFI-Nb2 and TNFI-Nb3.

values of 12 and 13, respectively (Figure 4). Of the peptides identified for TNFI-Nb1, seven partially matched sequences in the TCED™ database (Table 3). Similarly, TNFI-Nb2's 13 binders included seven partial matches, and TNFI-Nb3's binders included eight partial matches to previously identified T cell epitopes (Table 2). The contribution of specific anchor positions to MHC class II binding follows the hierarchy: P1 > P9 > P7 ≥ P6 ≥ P4.[18,19]

A diverse array of therapeutic antibodies and non-human proteins were evaluated by Abzena using the iTope-AI platform, with results illustrated in Figure 4. TNFI-Nbs exhibited Total Scores and Hotspot Max values as low as those of the least immunogenic human monoclonal antibodies currently utilized in clinical therapy. In contrast, many of the human monoclonal antibodies assessed displayed scores more than double those of TNFI-Nbs. This comparison highlights the favorable immunogenicity profile of TNFI-Nbs, underscoring their strong potential for therapeutic applications in TNFα-mediated diseases.

### *In silico humanization and developability optimization of lead TNFI nanobodies*

The nanobody panel, comprising TNFI-Nb, TNFI-Nb2, and TNFI-Nb3, underwent comprehensive humanization and developability optimization using the machine learning

**Table 2.** Summary of non-germline 9-mer MHC class II-binding peptides for TNFI-Nbs exhibiting promiscuous binding.

| | P1 Anchor Position | Peptide Sequence | Position Risk Score | TCED™ Homology |
|---|---|---|---|---|
| **TNFI-Nb1** | 21 | SCAASGFAF | 1 | None |
| | 23 | AASGFAFND | 6 | None |
| | 27 | FAFNDHWMY | 7 | None |
| | 32 | HWMYWVRQA | 4 | -WM-WVRQA |
| | 35 | YWVRQAPGK | 5 | YWVRQAPGK |
| | 36 | WVRQAPGKE | 4 | W-RQAPGKE |
| | 37 | VRQAPGKEL | 1 | -RQAPGK-L |
| | 47 | WVSEINTNG | 1 | None |
| | 78 | TLYLQMDSL | 6 | None |
| | 79 | LYLQMDSLR | 2 | None |
| | 80 | YLQMDSLRP | 20 | YLQM-SLRP |
| | 81 | LQMDSLRPE | 6 | LQM-SLRPE |
| | 104 | LRGQGTQVT | 4 | None |
| | 106 | GQGTQVTVS | 5 | GQGTQVTVS |
| **TNFI-Nb2** | 21 | SCAASGFAF | 1 | None |
| | 23 | AASGFAFND | 6 | None |
| | 27 | FAFNDHWMY | 7 | None |
| | 32 | HWMYWVRQA | 4 | -WM-WVRQA |
| | 35 | YWVRQAPGK | 5 | YWVRQAPGK |
| | 36 | WVRQAPGKE | 4 | W-RQAPGKE |
| | 37 | VRQAPGKEL | 1 | -RQAPGK-L |
| | 47 | WVSEINTNG | 1 | None |
| | 79 | LYLQMNSLE | 1 | None |
| | 80 | YLQMNSLEP | 8 | YLQMNSL-P |
| | 81 | LQMNSLEPE | 12 | LQMNSL-PE |
| | 104 | LRGQGTQVT | 4 | None |
| | 106 | GQGTQVTVS | 5 | GQGTQVTVS |
| **TNFI-Nb3** | 21 | SCAASGFAF | 1 | SCAASGF-F |
| | 23 | AASGFAFND | 6 | None |
| | 27 | FAFNDHWMY | 7 | None |
| | 32 | HWMYWVRQA | 4 | -WM-WVRQA |
| | 35 | YWVRQAPGK | 5 | YWVRQAPGK |
| | 36 | WVRQAPGKE | 4 | W-RQAPGKE |
| | 37 | VRQAPGKEL | 1 | -RQAPGK-L |
| | 47 | WVSEINTNG | 1 | None |
| | 79 | LYLQMNSLE | 2 | None |
| | 80 | YLQMNSLEP | 9 | YLQMNSL-P |
| | 81 | LQMNSLEPE | 13 | LQMNSL-PE |
| | 104 | LRGQGTQVT | 4 | None |
| | 106 | GQGTQVTVS | 5 | GQGTQVTVS |

Each peptide is presented with its $P_1$ anchor position, amino acid sequence, and position risk score. Homologous peptides identified in the TCED™ database are listed, with mismatched residues indicated by ( – ).

algorithm AbNatiV.[20] AbNatiV is a recently introduced AI framework that can accurately predict both humanness and VHH-nativeness of nanobodies from the sequence alone. Humanness scores greater than 0.8 correspond to typically human variable-domain sequences, thereby minimizing potential immunogenicity, while scores below 0.8 indicate non-human origins, which is associated with a higher likelihood of immunogenicity. Among the three nanobodies, TNFI-Nb was selected as the optimal starting wild-type (WT) for humanization based on its superior initial humanness and CamSol solubility scores,[20] coupled with robust VHH-nativeness (Table 4).

Two distinct mutational sampling strategies were used: enhanced sampling, which iteratively explores the mutational landscape to rapidly converge on a single humanized sequence, and exhaustive sampling, which systematically assesses all permissible mutation combinations within the position-specific scoring matrices (PSSMs) of human VH and nanobodies.[2] Both approaches identify optimal variants on the Pareto Front, maximizing humanness without compromising VHH-nativeness, which is important to retain stability and folding in the absence of a VL domain.[2] Importantly, humanization focused exclusively on solvent-exposed residues within the framework regions, and CDR regions were excluded to minimize the risk of hindering binding. We noted that both automated humanization pipelines suggested a mutation in the C-terminal stem of the CDR3 loop, which is an arginine in all TNFI-Nbs but is much more commonly a tryptophan in native nanobodies and human VH domains. Consequently, we hypothesized that a rare residue at this stem position next to the CDR3 loop may serve an important functional role, and we thus reverted it to WT arginine in some designs prior to experimental testing (Table 5).

As a further control for structural integrity post-humanization, the structures of WT and all humanized sequences were modeled with ImmuneBuilder.[21] The modeled structures were superimposed based on their framework regions, and the root-mean-square deviation (RMSD) calculated for the CDR regions was approximately 1Å. This value is significantly smaller than the expected modeling accuracy for these regions suggesting minimal or no displacement of the CDR loops because of the humanizing framework mutations.

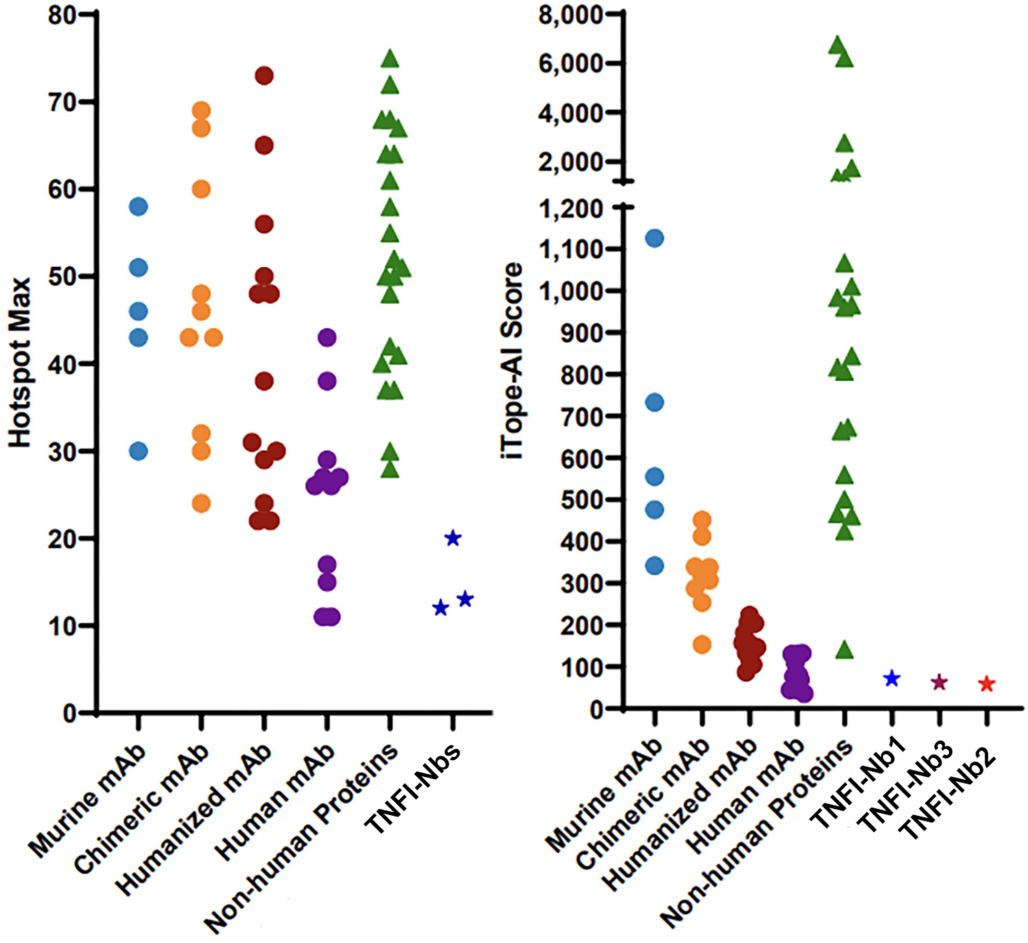


**Figure 4.** TNFI-Nb1, TNFI-Nb2 and TNFI-Nb3 have low predicted immunogenicity.

**Table 3.** Summary of TCED™ interrogation for non-germline binding peptides of TNFI-Nbs.

| | P1 Anchor Position | Peptide Sequence | TCED™ Homology | Residues Identical to TCED™ peptide | TCED™ Key Anchor Positions |
|---|---|---|---|---|---|
| **TNFI-Nb1** | 32 | HWMYWVRQA | -WM-WVRQA | 7/9 | 6, 7, 9 |
| | 35 | YWVRQAPGK | YWVRQAPGK | 9/9 | 1, 4, 6, 7, 9 |
| | 36 | WVRQAPGKE | W-RQAPGKE | 8/9 | 1, 4, 6, 7, 9 |
| | 37 | VRQAPGKEL | -RQAPGK-L | 7/9 | 4, 6, 7, 9 |
| | 80 | YLQMDSLRP | YLQM-SLRP | 8/9 | 1, 4, 6, 7, 9 |
| | 81 | LQMDSLRPE | LQM-SLRPE | 8/9 | 1, 6, 7, 9 |
| | 106 | GQGTQVTVS | GQGTQVTVS | 9/9 | 1, 4, 6, 7, 9 |
| **TNFI-Nb2** | 32 | HWMYWVRQA | -WM-WVRQA | 7/9 | 6, 7, 9 |
| | 35 | YWVRQAPGK | YWVRQAPGK | 9/9 | 1, 4, 6, 7, 9 |
| | 36 | WVRQAPGKE | W-RQAPGKE | 8/9 | 1, 4, 6, 7, 9 |
| | 37 | VRQAPGKEL | -RQAPGK-L | 7/9 | 4, 6, 7, 9 |
| | 80 | YLQMNSLEP | YLQMNSL-P | 8/9 | 1, 4, 6, 7, 9 |
| | 81 | LQMNSLEPE | LQMNSL-PE | 8/9 | 1, 4, 6, 9 |
| | 106 | GQGTQVTVS | GQGTQVTVS | 9/9 | 1, 4, 6, 7, 9 |
| **TNFI-Nb3** | 21 | SCAASGFAF | SCAASGF-F | 8/9 | 1, 4, 6, 7, 9 |
| | 32 | HWMYWVRQA | -WM-WVRQA | 7/9 | 6, 7, 9 |
| | 35 | YWVRQAPGK | YWVRQAPGK | 9/9 | 1, 4, 6, 7, 9 |
| | 36 | WVRQAPGKE | W-RQAPGKE | 8/9 | 1, 4, 6, 7, 9 |
| | 37 | VRQAPGKEL | -RQAPGK-L | 7/9 | 4, 6, 7, 9 |
| | 80 | YLQMNSLEP | YLQMNSL-P | 8/9 | 1, 4, 6, 7, 9 |
| | 81 | LQMNSLEPE | LQMNSL-PE | 8/9 | 1, 4, 6, 9 |

Homologous peptides identified from the TCED™ database that match the anchor position hierarchy ($P_1 > P_9 > P_7 \geq P_6 \geq P_4$) are listed.

Following in silico humanization, we used the structural models of both Enhanced and Exhaustive humanized variants as inputs for the CamSol Combination pipeline,[22] by excluding all CDR regions from the design and by using an alignment of human VH sequences as input. CamSol Combination automatically identifies combinations of mutations predicted to improve solubility and conformational stability, or one of these properties without affecting the other. The apparent melting temperature of in silico mutants was predicted with NanoMelt.[22] Of the mutations

**Table 4.** AbNatiV assessment of TNFI-Nbs.

| ID | Sequence | | | | | | |
|---|---|---|---|---|---|---|---|
| 1 | EVQLVESGGGLVQPGGSLRLSCAAS | GFAFNDHWMY | WVRQAPGKELEWVS | EINTNGLITK | YADFVKGRFTVSRDNAKNTLYLQMDSLRPEDTAVYSCS | RNQIGTL | RGQGTQVTVSS |
| 2 | QVQLVESGGGLVQPGGSLRLSCAAS | GFAFNDHWMY | WVRQAPGKELEWVS | EINTNGLITK | YADFVKGRFTVSRDNAKNTLYLQMNSLEPEDTAVYSCS | RNQIGTL | RGQGTQVTVSS |
| 3 | QVQLVESGGGLVQPGGSLRLSCAAS | GFAFNDHWMY | WVRQAPGKELEWVS | EINTNGLITK | YADFVKGRFTVSRDNAENTLYLQMNSLEPEDTAVYSCS | RNQIGTL | RGQGTQVTVSS |

| | **Name** | **Humanness** | **VHH-nativeness** | **Intrinsic Solubility** |
|---|---|---|---|---|
| 1 | TNFI-Nb1 | 0.780 | 0.822 | 0.947 |
| 2 | TNFI-Nb2 | 0.761 | 0.837 | 0.795 |
| 3 | TNFI-Nb3 | 0.755 | 0.838 | 0.807 |

CDRs are highlighted with gray shading. Key evaluation metrics include humanness (H), VHH-nativeness (V), and CamSol intrinsic solubility scores (S). Based on the highest humanness and solubility scores, TNFI-Nb1 was selected for the derivation of optimized mutant nanobodies.

**Table 5.** TNFI-Nb1 mutants with enhanced therapeutic potential determined by in-silico analysis.

| ID | Sequence |
|---|---|
| WT | EVQLVESGGGLVQPGGSLRLSCAASGFAFNDHWMYWVRQAPGKELEWVSEINTNGLITKYADFVKGRFTVSRDNAKNTLYLQMDSLRPEDTAVYSCSRNQIGTLRGQGTQVTVSS |
| 1 | EVQLVESGGGLVQPGGSLRLSCAASGFAFNDHWMYWVRQAPGK**G**LEWVSEINTNGLITKYAD**S**VKGRFTVSRDNAKNTLYLQMDSLRPEDTAVYSCSRNQIGTLRGQGTQVTVSS |
| 2 | EVQLVESGGGLVQPGGSLRLSCAASGFAFNDHWMYWVRQAPGK**G**LEWVSEINTNGLITKYAD**S**VKGRFTVSRDNAKNTLYLQMDSLRPEDTAVYSCSRNQIGTL**W**GQGTQVTVSS |
| 3 | EVQLVESGGGLVQPGGSLRLSCAASGFAFNDHWMYWVRQAPGK**G**LEWVSEINTNGLITKYAD**S**VKGRFTVSRDN**S**KNTLYLQMDSLRPEDTAVYSCSRNQIGTLRGQGT**L**VTVSS |
| 4 | EVQLVESGGGLVQPGGSLRLSC**K**ASGFAFNDHWMYWVRQAPGK**G**LEWVSEINTNGLITKYAD**S**VKGRFTVSRDN**S**KNTLYLQMDSLRPEDTAVYSCSRNQIGTL**W**GQGT**L**VTVSS |
| 5 | EVQLVESGGGLVQPGGSLRLSCAASGFAFNDHWMYWVRQAPGK**G**LEWVSEINTNGLITKYAD**S**VKGRFTVSRDNAKNTLYLQMDSLRPEDTAVYSCSRNQIGTL**W**GQGT**L**VTVSS |

| ID | Design/clone name | Name | Humanness | VHH-nativeness | Intrinsic Solubility | Predicted $T_m$ |
|---|---|---|---|---|---|---|
| WT | 05C08 | TNFI-Nb1 | 0.780 | 0.822 | 0.947 | 63.35 |
| 1 | Enhanced CDR3_stem_intact | TNFI-α | 0.809 | 0.855 | 0.975 | 62.8 |
| 2 | Enhanced | | 0.823 | 0.861 | 0.830 | 63.4 |
| 3 | Enhanced CDR3_stem_intact v1 | TNFI-β | 0.826 | 0.836 | 1.047 | 62.4 |
| 4 | Enhanced v3 | | 0.816 | 0.814 | 0.956 | 64.1 |
| 5 | Exhaustive | | 0.847 | 0.842 | 0.846 | 63.6 |

Mutations are underlined and in bold. Numerical values in the columns are the humanness and VHH-nativeness scores predicted by AbNativ, the intrinsic sequence-based solubility score predicted by CamSol, and the apparent melting temperature predicted with NanoMelt. The mutation in red at the stem of the CDR3 region is a mutation that was suggested by both enhanced and exhaustive AbNativ automated sequence-based humanization pipelines. This fact is not surprising as the WT arginine residue is very rare at this position in natural nanobodies, and in fact the mutation to the much more common tryptophan increases both humanness and VHH-nativeness (and predicted melting temperature slightly). However, we hypothesized that a rare residue at the stem of the CDR3 may play an important functional role in binding to the target, and therefore we reverted it to WT in all 'stem_intact' designs. Indeed, R is also present at this position in TNFI-Nb2 and TNFI-Nb3, further supporting its functional relevance. The mutations in green in designs v1 and v3 were suggested by the CamSol combination pipeline as mutations predicted to increase solubility and/or stability, without reducing humanness (as assessed by AbNativ).

suggested by this approach, we retained only those that did not reduce humanness according to AbNativ scoring (Table 5).

In summary, 5 TNFI-Nb computationally designed variants were selected for experimental characterization (Table 5). Three of these had the R to W mutation in the stem of the CDR3 loop, while in the others this mutation was reverted to reduce the risk of disrupting binding. These designed variants were produced in CHO-S cells with production performed at GenScript, and detailed experimental procedures and results are provided in the Supporting information data file entitled: *Optimized TNFI-Nbs Production*.

### *Assessment of TNFα inhibitory activity in optimized TNFI-Nb mutants*

To evaluate the TNFI activity of the five TNFI-Nb1 mutants and compare it to that of TNFI-Nb1 on TNFα-induced apoptosis, we employed the IncuCyte Caspase-3/7 Activation Assay using the IncuCyte live-cell imaging system (Sartorius). This assay enables real-time kinetic monitoring of apoptotic events in living cells. WEHI-13VAR cells were treated with 0.25 ng/mL trimeric human TNFα and 1 μg/mL Actinomycin-D, either alone or with twofold serial dilutions of TNFI-Nbs (from 10,000 to 12.2 pM). Apoptosis was measured using a 0.5 μM Caspase-3/7 Green Reagent, which fluoresces upon caspase activation. $IC_{50}$ values represent the concentration of TNFI-Nb required to inhibit 50% of TNFα-induced caspase activity. Plates were placed in the IncuCyte system, which maintained optimal incubation conditions while capturing fluorescence images at 30-minute intervals. The 10-hour time point was selected to assess TNFI activity because caspase-3/7 activity induced by Actinomycin D alone was minimal, whereas activity induced by TNFα plus Actinomycin D was significantly elevated. This contrast allowed for more accurate measurements of the nanobodies' effects on TNFα-dependent caspase-3/7 activation. The IncuCyte software quantified fluorescence intensity, correlating to caspase-3/7 activity and thereby apoptotic cell death. Data were normalized to control wells treated with Actinomycin-D alone. The concentration of each nanobody required to achieve 50% inhibition of caspase-3/7 activation ($IC_{50}$), compared to the wells treated with TNFα plus Actinomycin D only, was calculated.

The IncuCyte Caspase-3/7 activation assays revealed varying inhibitory activities among the tested nanobody mutants against TNFα-induced caspase-3/7 activation. The Enhanced, Enhanced v3, and Exhaustive mutants exhibited $IC_{50}$ values of 1.417 nM, 29.896 nM, and 2.27 nM, respectively, indicating reduced potency compared to the parental TNFI-Nb1 ($IC_{50}$ = 133.5 pM). This reduction in potency is likely attributable to the W to R mutation at the stem of the CDR3 region. In contrast, the Enhanced CDR3_stem_intact and CDR3_stem_intact v1 mutants, which lack this mutation, demonstrated significantly improved $IC_{50}$ values of 48.84 pM and 64.31 pM, respectively, reflecting enhanced inhibitory activity against TNFα. For simplicity, Enhanced CDR3_stem_intact and CDR3_stem_intact v1 have been renamed TNFI-α and TNFI-β, respectively (Figure 5a,b). These optimized mutants, TNFI-α and TNFI-β, exhibit superior inhibitory performance, underscoring their strong potential for clinical development by offering increased efficacy alongside a reduced likelihood of anti-drug antibody formation.

### *SPR analysis of TNFI-α and TNFI-β binding to human TNFα*

To evaluate the binding affinities of TNFI-α and TNFI-β to human TNFα, SPR analysis was performed. The purity of the nanobody samples, TNFI-α and TNFI-β, along with human TNFα, was confirmed to exceed 90%, ensuring high-quality reagents for analyses. Assay development and kinetic analysis were conducted using Cytiva's Biacore 1K SPR system with Carboxyl CM5 sensors. This process involved optimizing immobilization conditions, buffer formulations, regeneration protocols, and kinetic fitting models to establish reliable and reproducible measurement conditions. Optimal

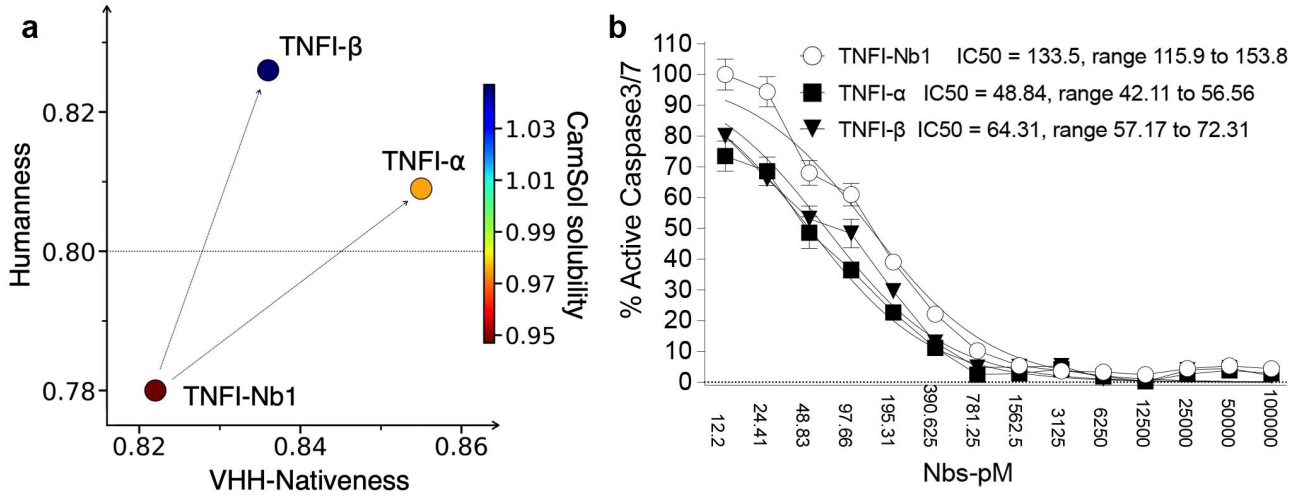


**Figure 5.** In silico engineering of TNFI-α and TNFI-β nanobodies: optimized mutants of TNFI-Nb1 with enhanced TNFI activity.

immobilization was achieved at a ligand concentration of 2.5 µg/mL in 10 mm acetate buffer (pH 4.5), resulting in response maxima (Rmax) of 34.44 RU for TNFI-α and 12.74 RU for TNFI-β, aligning with theoretical predictions. Buffer optimization identified 1× PBS supplemented with 3 mM EDTA and 0.05% v/v Surfactant P20 as the optimal running buffer, minimizing nonspecific binding and maximizing signal-to-noise ratios.

Kinetic analysis revealed that the interactions between TNFα and both nanobodies adhered to a 1:1 binding model (Figure 6a), with KD of 167 pM for TNFI-α and 405 pM for TNFI-β (Figure 6b), indicating high affinity binding. Iso-affinity analysis further demonstrated that TNFI-α exhibited a significantly faster association rate (ka) compared to TNFI-β, contributing to its superior overall binding affinity (Figure 6c). These results indicate that TNFI-α and TNFI-β exhibit high affinity for TNFα, comparable to the affinities observed for TNFI-Nb1, TNFI-Nb2, and TNFI-Nb3, underscoring the potential of TNFI-α and TNFI-β as highly effective therapeutic agents targeting TNFα-mediated pathways. The binding kinetics of TNFI-Nb1, TNFI-Nb2, TNFI-Nb3, and TNFI-α/TNFI-β were measured using two different SPR systems: Nicoya's OpenSPR and Cytiva's Biacore K, respectively. While the relative response unit (RU) scales and maximal RU levels differ between the systems (Table 6 and Supplementary Figures S9 and S10), the absolute kinetic parameters remain consistent and independent of the platform. All SPR experiments were conducted at Rapid Novor.

As summarized in Table 5, the humanization process yielded two nanobodies with enhanced humanness scores without compromising their biological activity, specifically TNFα inhibition. In fact, the activity of the humanized nanobodies appears to be slightly enhanced. TNFI-α demonstrated the lowest IC50 value (48.84 pM) compared to TNFI-β (64.3 pM), indicating superior inhibitory activity. However, TNFI-β exhibited higher humanness (0.826 vs. 0.809) and solubility (1.047 vs. 0.975) scores. These complementary strengths make both TNFI-α and TNFI-β strong candidates for further development.

### *Comparative analysis of TNFI-β against previously described anti-TNFα VHHs*

To contextualize the novelty and therapeutic relevance of our TNFI-Nbs, we performed a comparative structural and sequence analysis with previously characterized VHHs. This included Llama VHH1, VHH2, and VHH3, with corresponding PDB codes 5M2I, 5M2J, and 5M2M, which exhibit $IC_{50}$ values of 242 pM, 748 pM, and 1.503 nM, and KD of 540 pM, 130 pM, and 1.5 nM, respectively.[23] We also compared our nanobodies to ozoralizumab (Nanozora®), a trivalent TNFα inhibitor composed of two anti-TNFα VHHs and an albumin-binding VHH for half-life extension[4,24,25] that is marketed as a treatment for rheumatoid arthritis in Japan. Ozoralizumab (PDB code: 8Z8M) has been reported to exhibit an $IC_{50}$ of 12 pM in cell-based assays and a KD of 20.2 pM for human TNFα. However, it should be noted that these values reflect the affinity and potency of the trivalent construct. This comparative analysis should be considered approximate, as our experimentally determined $IC_{50}$ values are compared to data reported in the literature. A key limitation of this comparison is that $IC_{50}$ values obtained at different times, in different laboratories, and using varying assay conditions or readout systems are not always comparable. Nevertheless, we present these values with this caveat in mind, as they still provide useful context and may offer the reader a general sense of relative inhibitory potency.

Comparison of TNFI-β to 5M2I, 5M2J, 5M2M, and 8Z8M at both the overall and CDR sequence levels reveals that 8Z8M is most similar to TNFI-β, closely followed by 5M2J (Tables 7 and 8). Notably, 5M2J and 8Z8M are nearly identical, with an overall sequence identity of 95.65%, 99.13% similarity, and no alignment gaps.

### *TNFI-α binds to plasma-membrane human TNFα*

To assess whether humanized nanobodies bind to membrane-bound human TNFα, we conducted an experiment using transfected cells expressing human TNFα or mouse

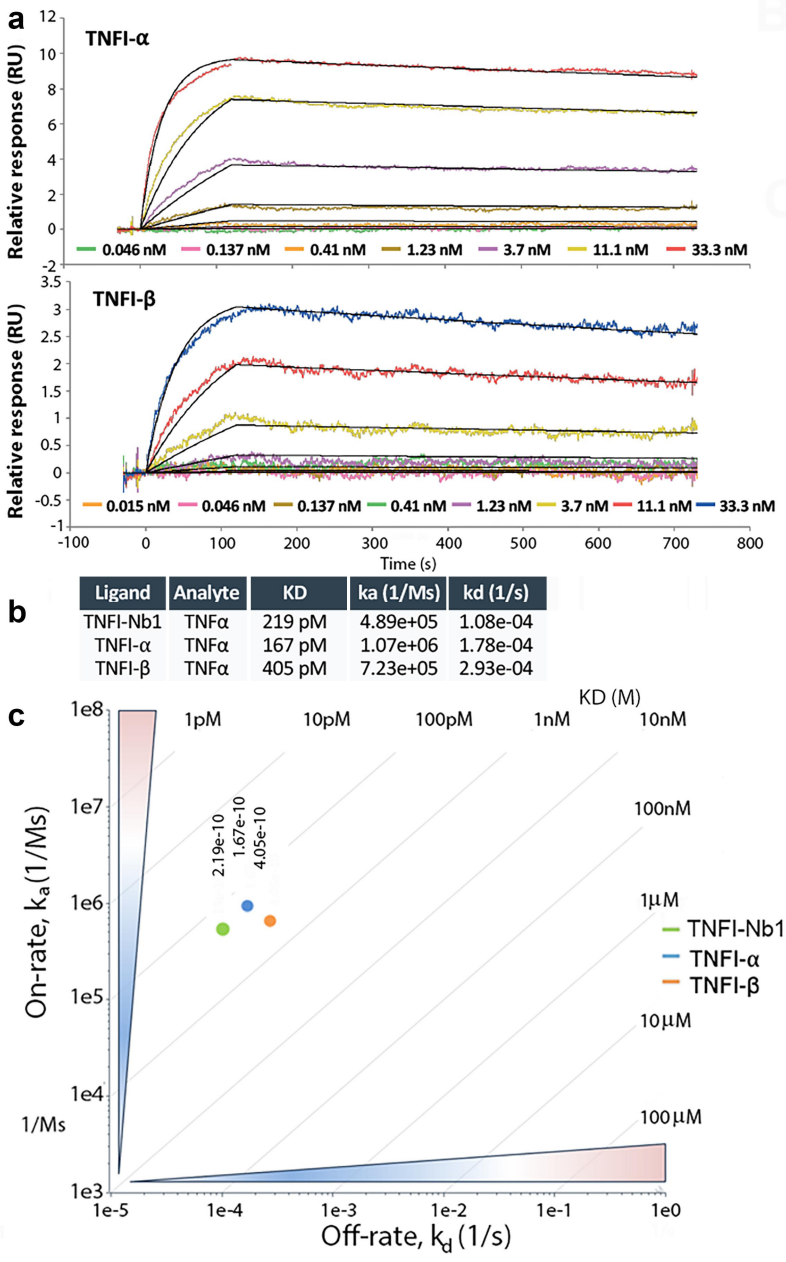


**Figure 6.** Kinetics of TNFα analytes binding to immobilized nanobodies.

**Table 6.** Absolute ligand immobilization values (RL) across SPR platforms.

| | TNFI-Nb1 | TNFI-Nb2 | TNFI-Nb3 | TNFI-α | TNFI-β |
|---|---|---|---|---|---|
| $R_L$ | 403 RU | 478 RU | 378 RU | 7.30 RU | 2.70 RU |

To evaluate the binding kinetics of TNFI-Nb1, TNFI-Nb2, and TNFI-Nb3 compared to TNFI-α and TNFI-β, we utilized two different SPR systems: Nicoya's OpenSPR and Cytiva's biacore K. While both systems accurately determine kinetic parameters, they differ in biosensor properties and SPR measurement principles. OpenSPR employs 100 nm gold nanoparticles with an evanescent field of ~ 20 nm, whereas biacore K utilizes 2D planar gold sensors with an evanescent field of ~ 200 nm. These differences influence signal properties and ligand immobilization requirements. OpenSPR minimizes bulk shift and reduces buffer-related signal interference but requires higher ligand immobilization. In contrast, biacore K may exhibit a higher bulk shift but requires significantly less ligand immobilization on the sensor surface. As a result, relative response unit (RU) scales and maximal RU levels differ between the two systems. However, with appropriate experimental setup, absolute kinetic parameters remain universal and independent of the SPR platform.

**Table 7.** Sequence identity, similarity, and gap percentages between TNFI-β and previously characterized anti-TNFα nanobodies 5M2I, 5M2J, 5M2M, and 8Z8M.

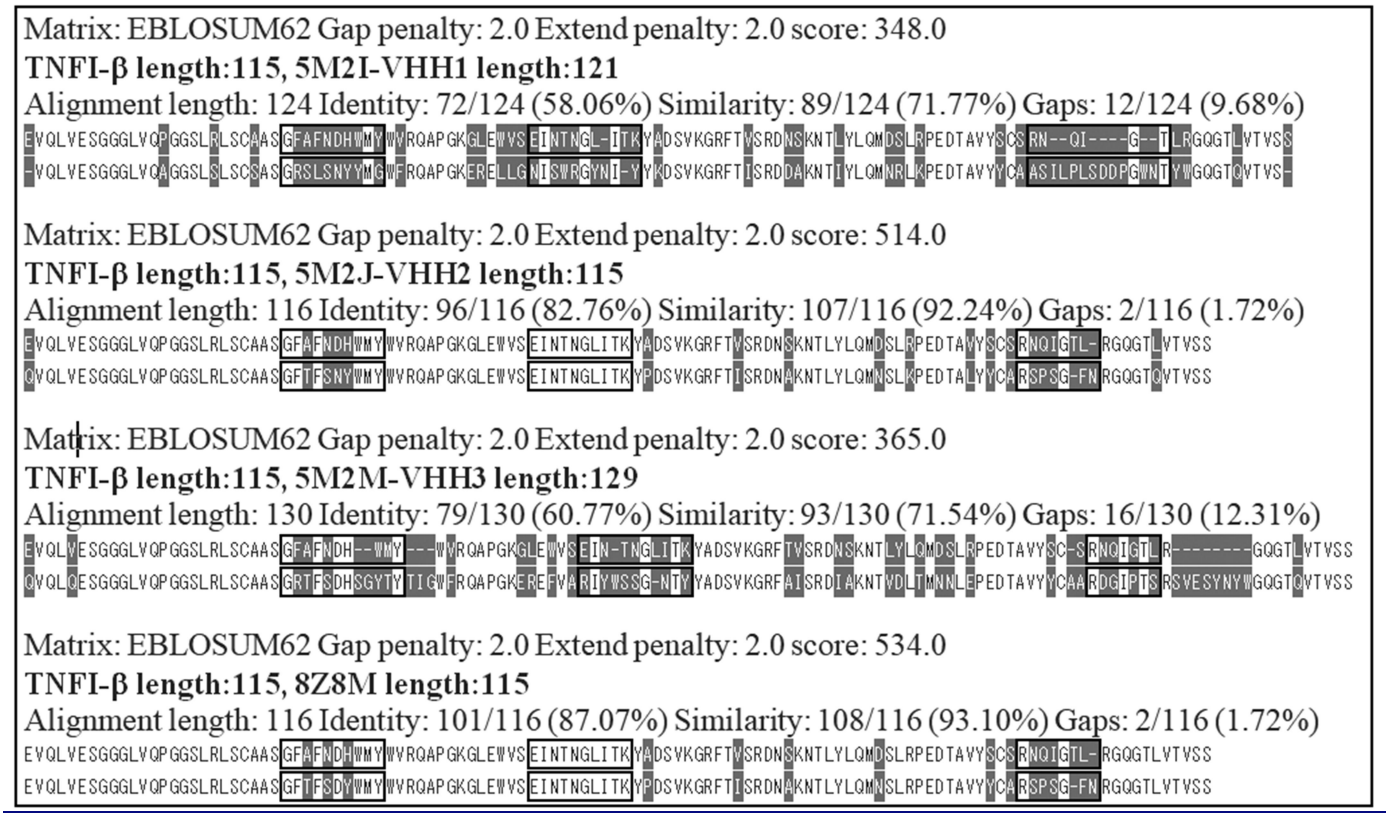


CDR-level comparisons highlight that CDR2 is identical across TNFI-β, 5M2J, and 8Z8M, while CDR1 and CDR3 show lower degrees of similarity. 8Z8M exhibits the highest overall similarity to TNFI-β, with 5M2J and 8Z8M being nearly identical to each other.

**Table 8.** Overall and CDR sequence identity and similarity between TNFI-β and 5M2I, 5M2J, 5M2M, and 8Z8M.

| | Overall | | CDR1 | | CDR2 | | CDR3 | |
|---|---|---|---|---|---|---|---|---|
| | Identity | Similarity | Identity | Similarity | Identity | Similarity | Identity | Similarity |
| 5M2I | 58.06% | 71.77% | 20% | 70% | 27.27% | 36.36% | 14.29% | 21.43% |
| 5M2J | 82.76% | 92.24% | 60% | 90% | **100%** | | 28.57% | 42.86% |
| 5M2M | 60.77% | 71.54% | 41.67% | 58.33% | 27.27% | 45.45% | 42.86% | 57.14% |
| 8Z8M | 87.07% | 93.1% | 60% | 80% | **100%** | | 28.57% | 42.86% |

TNFα as control (Figure 7). To exclude nonspecific binding due to compromised membranes, propidium iodide (PI)-positive cells were gated out. An anti-human TNFα antibody selectively stained cells transfected with a plasmid encoding human TNFα, but not those expressing mouse TNFα. Conversely, an anti-mouse TNFα antibody stained cells expressing mouse TNFα but not human TNFα. These results confirm that both antibodies bind only extracellular epitopes as staining was restricted to the appropriate transfectants, further indicating intact plasma membrane integrity. Both TNFI-α and TNFI-Nb1 specifically stained cells expressing human TNFα, particularly those with higher EGFP fluorescence, consistent with stronger transgene expression. In contrast, they showed minimal binding to cells expressing mouse TNFα, confirming their higher affinity for human TNFα. These findings demonstrate that TNFI nanobodies selectively recognize membrane-bound human TNFα in a transfection-based assay.

TNFI-α and TNFI-β, respectively, have been assigned by NanoNewron commercial designations as follows: TNFI-α: NN-223; TNFI-β: NN-224. Both NN-223 and NN-224 are currently under evaluation for further preclinical development. These variants represent promising candidates for therapeutic applications targeting human TNFα.

## Discussion

In this study we present the generation, characterization, and optimization of TNFI-Nbs NN-223 and NN-224. Through humanization and functional optimization, NN-223 (formerly TNFI-α) and NN-224 (formerly TNFI-β) emerged as lead candidates, exhibiting enhanced predicted humanness and solubility coupled with slightly improved measured TNFα inhibitory activity. These findings underscore the efficacy of nanobody engineering in producing biologics with superior therapeutic profiles. For clarity, these nanobodies will be referred to by their commercial names, NN-223 (TNFI-α) and NN-224 (TNFI-β), throughout the remainder of this discussion.

The manufacturing process for these nanobodies, achieved through transient transfection in CHO-S cells, yielded high purity and very low endotoxin levels. These attributes indicate that the production process is scalable for clinical applications.

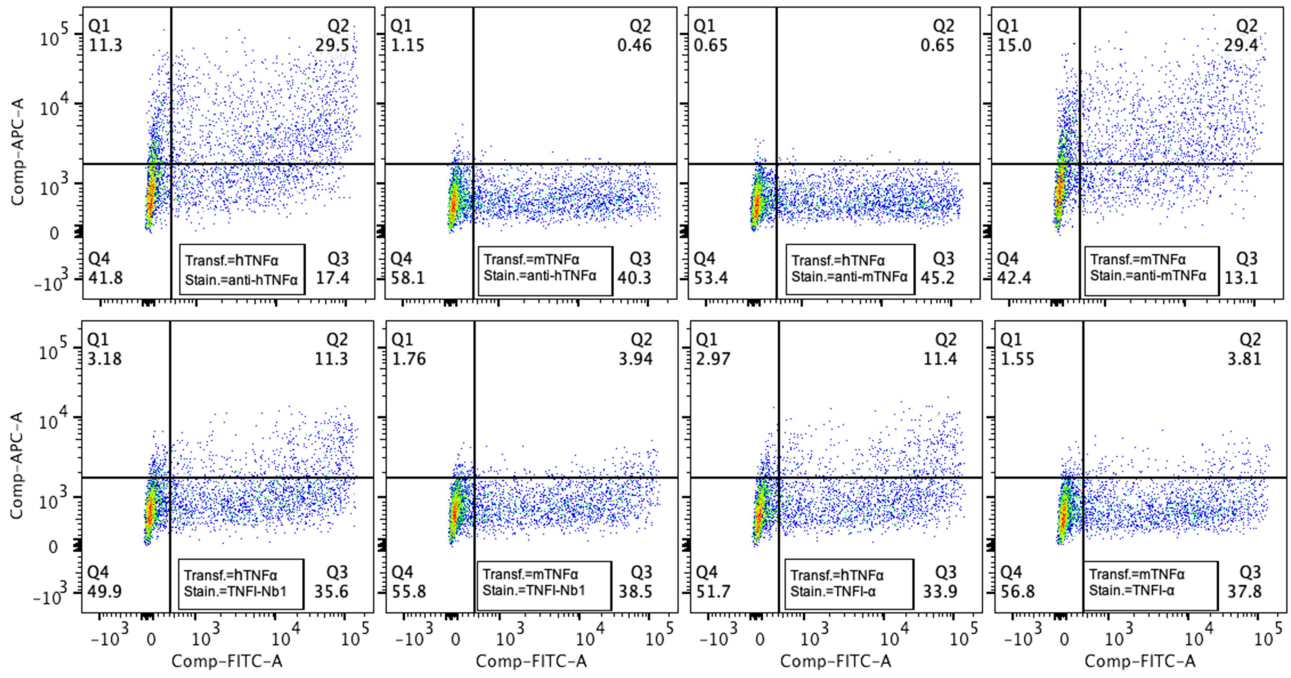


**Figure 7.** Humanized TNFI-α binds to membrane-bound human TNFα in a transfection model.

SPR analysis confirmed that both NN-223 (TNFI-α) and NN-224 (TNFI-β) maintain high binding affinities for soluble human TNFα, with KD values of 167 pM and 405 pM, respectively. These affinities are comparable to those of earlier TNFI-Nb prototypes (TNFI-Nb1, TNFI-Nb2, and TNFI-Nb3). The ability of NN-223 (TNFI-α) and NN-224 (TNFI-β) to retain high affinity following humanization demonstrates the effectiveness of framework optimization strategies in minimizing immunogenic potential while preserving critical antigen-binding regions.

Functional assays assessing TNFα-induced caspase-3/7 activation revealed significantly improved $IC_{50}$ values for NN-223 (TNFI-α) and NN-224 (TNFI-β) compared to TNFI-Nb1. Specifically, NN-223 (TNFI-α) exhibited the most potent inhibitory activity with an $IC_{50}$ of 48.84 pM, while NN-224 (TNFI-β) achieved an $IC_{50}$ of 64.31 pM. These enhanced inhibitory efficacies, combined with favorable production parameters, bolster the clinical development potential of both nanobodies by offering superior efficacy alongside a reduced likelihood of anti-drug antibody formation.

Among the structurally characterized anti-TNFα nanobodies, NN-224 (TNFI-β) appears more closely related to 5M2J and 8Z8M than to 5M2I or 5M2M, based on overall sequence identity and similarity. However, notable differences in the CDRs suggest functional divergence. Among the three CDRs, CDR3 is typically the most critical for antigen recognition due to its length, structural variability, and central role in forming the antigen-binding interface. This is particularly true for VHH nanobodies, where CDR3 often dominates interactions with the target epitope. While NN-224 (TNFI-β) shares 100% identity in CDR2 with both 8Z8M and 5M2I, it exhibits lower similarity in CDR1 and especially CDR3, where identity drops to 25% with both nanobodies. Although structural studies to resolve the NN-224 (TNFI-β)/TNFα complex are still in progress, these CDR differences strongly suggest that NN-224 (TNFI-β engages TNFα via a distinct binding mode, potentially recognizing a different epitope or orientation compared to 8Z8M and 5M2I.

The therapeutic efficacy of TNFIs in diseases like rheumatoid arthritis, Crohn's disease, and psoriasis illustrates the ability of TNFα inhibition to significantly reduce systemic inflammation, even in conditions where other cytokines contribute to the inflammatory milieu.[1–5] This highlights TNFα's central role in modulating global inflammatory responses. However, US Food and Drug Administration-approved TNFI biologics, the most potent and specific TNFIs, have limited BBB permeability (CSF/Serum ratios ~ 0.001), which restricts their use in therapy of neuroinflammatory disorders, such as Alzheimer's disease (AD).[26–30] Emerging evidence from both human and animal studies implicates TNFα as a pivotal factor in AD pathogenesis.[31,32] Several findings highlight TNFα's role and its potential as a therapeutic target in AD.

## *Human evidence*

Elevated levels of TNFα have been consistently observed in the blood, cerebrospinal fluid (CSF), and CNS of AD patients.[33–37] These elevated TNFα levels are associated with increased neuroinflammation and are implicated in disease progression through both inflammatory and non-inflammatory mechanisms. Genetic studies have identified polymorphisms in TNFα and its receptors that are associated with increased AD risk,[38,39] suggesting that these variants may modulate TNFα expression or receptor activity, thereby amplifying its pathological impact.

Microglia, the primary producers of TNFα in the CNS, play a crucial role in AD pathogenesis.[40] Genetic studies have linked microglia-specific genes, such as TREM2, to late-onset AD

(LOAD).[41,42] Pathogenic variants like TREM2 p.R47H impair essential microglial functions, including phagocytosis and regulation of TNFα production, thereby exacerbating neuroinflammation and neuronal damage.

Clinical evidence supports the therapeutic potential of TNFα inhibition. Patients with inflammatory diseases treated with TNFIs exhibit a reduced risk of developing AD.[43,44] Additionally, peri-spinal and intrathecal administration of TNFIs, such as etanercept and infliximab, has shown cognitive improvements in sporadic AD cases.[45,46] These observations suggest that TNFα inhibition can mitigate neuroinflammation and associated cognitive decline in AD.

### Mechanistic insights from model organisms and in vitro studies

Elevated TNFα levels promote amyloid-beta (Aβ) production and impair its clearance, primarily through microglial dysfunction.[47] Deletion of TNF receptor 1 (TNFR1) in AD mouse models reduces Aβ formation and alleviates learning and memory deficits.[48] Furthermore, TNFα regulates synaptic receptor trafficking by promoting AMPA receptor export and GABA receptor import. Supraphysiological TNFα disrupts this balance, favoring excitatory dominance, impairing long-term potentiation (LTP), and increasing excitotoxicity risk.[49–51] As Aβ production and tau secretion are activity-dependent processes,[52–54] TNFα-driven excitatory activity may exacerbate both Aβ and tau pathology.

Data from *Trem2*$^{R47H}$ knock-in (KI) rats, a model for Late Onset AD, provide support for TNFα's role in AD pathogenesis. These KI rats exhibit early and significant increases in TNFα levels in the CNS and CSF. Elevated TNFα disrupts the excitatory/inhibitory balance, increases excitatory transmission, and reduces inhibitory transmission, thereby impairing LTP and exacerbating excitotoxicity. Administration of low doses of an anti-TNFα antibody with TNFI activity reverses these deficits, restoring excitatory/inhibitory balance, normalizing LTP, and mitigating the harmful effects of TNFα dysregulation.[55–57]

### Advantages of nanobodies over traditional biologic TNFIs

Unlike larger TNFI biologics, the smaller size and robust structural stability of nanobodies may facilitate better BBB penetration,[8,9] enhancing their therapeutic reach within the brain. Furthermore, nanobodies can be engineered for improved BBB permeability through strategies such as receptor-mediated transcytosis via TfR1,[10–13] potentially increasing their efficacy in treating neurodegenerative disorders. Thus, future studies will focus on evaluating the in vivo efficacy of NN-223 (TNFI-α) and NN-224 (TNFI-β), their pharmacokinetics, and their ability to cross the BBB, which would enable their use in CNS diseases linked to TNFα dysregulation. Comparative analyses in preclinical models will also help determine their relative suitability for clinical development based on efficacy, pharmacokinetics, and immunogenicity.

In conclusion, NN-223 (TNFI-α) and NN-224 (TNFI-β) represent significant advancements in nanobody engineering, offering high specificity, strong inhibitory activity, and favorable developability profiles. These optimized nanobodies demonstrate their potential as next-generation therapeutics for diseases driven by dysregulated TNFα signaling, including CNS inflammatory disorders such as AD. The combination of enhanced inhibitory efficacy, scalable manufacturing processes, and reduced immunogenic potential positions NN-223 (TNFI-α) and NN-224 (TNFI-β) as promising candidates for clinical development.

## Experimental procedures

### Antibodies and reagents

WEHI-13VAR cells (ATCC, CRL-2168) and HEK293T cells (ATCC, CRL-3216) were utilized in this study. Detailed information for the mammalian expression plasmids for human TNFα and EGFP (VB220203-1058zds) and mouse Tnfα and EGFP (VB220203-1060sqn) can be found here: https://en.vectorbuilder.com/vector/VB220203-1058zds.html. and https://en.vectorbuilder.com/vector/VB220203-1060sqn.html. The anti-His tag allophycocyanin (APC)-conjugated antibody was purchased from R&D Systems (Catalog No. IC050A). The APC-conjugated anti-human TNFα and anti-mouse TNFα antibodies were purchased from BioLegend (catalog numbers 502,912 and 506,107, respectively). Fugene transfection reagent was acquired from Promega (Catalog No. E2311). Recombinant human TNFα protein was sourced from Acro Biosystems (Catalog No. TNA-H5228), recombinant mouse TNFα protein from Acro Biosystems (Catalog No. TNA-M82E9), and recombinant rat TNFα protein from R&D Systems (Catalog No. 510-RT-010/CF). Fetal bovine serum (FBS) was obtained from Gibco (Catalog No. A3840102). EDTA was purchased from Sigma-Aldrich (Catalog No. N6507). PI was acquired from Invitrogen (Catalog No. P3566). DMEM and RPMI 1640 media were purchased from Corning (Catalog Nos. 10–017-CV and 10–040-CV, respectively). Acridine orange (AO)/PI staining solution was obtained from DeNovix (Catalog No. CD-AO-PI-7.5). Cell Counting Kit 8 (CCK-8) was sourced from DojinDo (Catalog No. CK-04). Actinomycin-D was acquired from Sigma-Aldrich (Catalog No. A9415), and Caspase-3/7 green dye was purchased from Thermo Fisher Scientific (Catalog No. C10423).

### Generation and screening of camelid anti-TNFα nanobodies

To generate anti-TNFα nanobodies (a-TNFα-Nabs), one alpaca and one llama were immunized with active trimeric human TNFα (Acro Biosystems, TNA-H5228). The immunization protocol began with an initial subcutaneous injection of 0.5 mg TNFα mixed with Complete Freund's Adjuvant (CFA) at week 0, followed by booster injections of 0.5 mg TNFα with Incomplete Freund's Adjuvant (IFA) every two weeks up to week 14. Serum samples were collected before immunization and at designated time points to assess antibody titers via ELISA, utilizing TNF-alpha-coated plates with appropriate negative and positive controls to ensure specificity.

At weeks 10 and 14, 500 mL of whole blood were drawn from each llama. PBMCs were isolated within four hours of blood collection using density gradient centrifugation, ensuring cell viability above 99% as determined by trypan blue exclusion. Total RNA was extracted from the isolated PBMCs using the RNeasy Maxi Kit (Qiagen) and quantified by

spectrophotometry, ensuring an A300/A280 ratio greater than 1.9. High-quality RNA was confirmed by agarose gel electrophoresis, displaying distinct 18S and 28S rRNA bands without signs of degradation. Complementary DNA (cDNA) was synthesized from the purified RNA using the SuperScript IV First-Strand Synthesis System (Thermo Fisher Scientific). A nanobody-specific library was constructed by amplifying the variable regions of heavy-chain-only antibodies (VHH) through a two-step PCR process using camelid-specific degenerate primers. The amplified VHH fragments were cloned into the pADL-20c phagemid vector using SfiI restriction sites and transformed into *E. coli* TG1 cells, resulting in a phage display library containing approximately $2.57 \times 10^9$ individual clones. Library diversity was confirmed by sequencing 74 random clones, which revealed 88% contained VHH inserts with intact open reading frames and no duplicate sequences. Library panning was performed against immobilized TNFα through three rounds of selection to enrich for specific binders. To reduce nonspecific interactions, the phage pool was pre-absorbed on bovine serum albumin (BSA)-coated wells before each panning round. Enrichment of specific phage binders was monitored using dot assays, which demonstrated increased binding to TNFα with each successive round.

Following panning, 94 individual clones were screened using an off-phage ELISA to identify those with specific binding to TNFα and minimal binding to BSA. Positive clones were further validated through repeat screening and sequencing to ensure specificity and diversity. Selected nanobodies were expressed in a non-amber-suppressor strain of *E. coli*, and periplasmic fractions containing His-tagged nanobodies were purified using His-tag affinity chromatography. Purity was confirmed by SDS-PAGE, and nanobody concentrations were determined by absorbance at 280 nm. Purified nanobodies were dialyzed into PBS (pH 7.4) and filter-sterilized for downstream applications. A detailed summary of Abcore's experimental procedures is provided in the Supporting information data file entitled: Identification, Cloning, and Production of α-TNFα-Nabs.

### Production of nanobodies in CHO-S cells

Protein production was performed by GenScript, and detailed experimental procedures and results are provided in the Supporting information data files entitled: TNFI-Nb Production in CHO-S cells and Optimized TNFI-Nbs Production.

### SPR analyses

These analyses were performed by Rapid Novor. The purity of the nanobodies, as well as human TNFα, was confirmed to exceed 90%, ensuring high-quality reagents for subsequent assays. Kinetic analyses were performed using Cytiva's Biacore 1K SPR system and Nicoya's OpenSPR-XT instrument with Carboxyl CM5 sensors.

### In-silico immunogenicity prediction

Immunogenicity risk of TNFI-Nabs was evaluated using the iTope-AI platform in conjunction with the TCED™ database. The analysis was performed by Abzena. Details of experimental procedures are provided in the Supporting information data files entitled: iTope analysis of TNFI-Nb1–3 immunogenicity.

### TNFI activity and $IC_{50}$ determination assays

WEHI 13VAR cells were cultured in RPMI 1640 medium supplemented with 10% FBS in a humidified incubator maintained at 37°C with 5% $CO_2$. Cells were harvested, and cell number and viability were assessed using AO/PI staining with a Denovix Celldrop cell counter. The cell suspension was adjusted to a density of 30,000 cells per well, and 90 µL of this suspension was seeded into a 96-well plate containing RPMI 1640 medium with 10% FBS and 1 µg/mL Actinomycin-D. Nanobodies were pre-mixed at serial concentrations with human TNFα active trimer, mouse TNFα active trimer, or rat TNFα active trimer and incubated at room temperature for 30 minutes. Subsequently, 10 µL of the pre-mixed solution was added to each well containing WEHI 13VAR cells, resulting in a final TNF-α concentration of 0.25 ng/mL and the desired final concentrations of Nbs.

The cytotoxicity assay was conducted by incubating the plates for 24 hours at 37°C with 5% $CO_2$. Following incubation, 10 µL of Cell Counting Kit 8 (CCK-8) was added to each well, and the plates were incubated for an additional 2–4 hours. Absorbance was measured at 450 nm using a microplate reader. To quantify TNFα-induced cytotoxicity, cytotoxicity values from wells treated with Actinomycin-D alone were subtracted from those treated with both Actinomycin-D and TNFα. The percentage protection conferred by TNFI-Nbs was calculated by setting the cytotoxicity induced by Actinomycin-D plus TNFα as 100%, and expressing the cytotoxicity of samples treated with Actinomycin-D, TNFα, and TNFI-Nbs as a percentage of this reference value.

For the Caspase-3/7 activity assays, cells were treated as described above with one modification: Caspase-3/7 dye was added to the pre-mixed solution containing TNFα, and nanobodies to achieve a final concentration of 0.5 µM upon addition to the cells. The plate was monitored using the IncuCyte live-cell analysis system, maintaining incubation at 37°C with 5% $CO_2$. To quantify TNFα-induced Caspase-3/7 activity, activity values from wells treated with Actinomycin-D alone were subtracted from those treated with both Actinomycin-D and TNFα. The percentage protection conferred by TNFI-Nbs was calculated by setting the Caspase-3/7 activity induced by Actinomycin-D plus TNFα as 100% and expressing the Caspase-3/7 activity of samples treated with Actinomycin-D, TNFα, and TNFI-Nbs as a percentage of this reference value.

### FACS analysis

HEK293T cells were cultured in DMEM medium supplemented with 10% FBS in a humidified incubator maintained at 37°C with 5% $CO_2$. HEK293T cells were transiently transfected with constructs encoding human TNFα and EGFP using Fugene transfection reagent and incubated for 24 hours. Transfected cells were harvested and resuspended in ice-cold FACS buffer (PBS supplemented with 1% BSA and 1 mm EDTA, pH 7.2). Nanobodies were added to the cells in a 96-well plate and incubated at 4°C with shaking for 45 minutes.

Following incubation, cells were centrifuged at 1000 × g for 5 minutes and washed three times with 200 µL of FACS buffer. The cell pellet was then resuspended in 100 µL of FACS buffer containing anti-His tag APC-conjugated antibody at a 1:100 dilution and incubated for 30 minutes at 4°C with shaking. After another centrifugation at 1000 × g for 5 minutes and three additional washes with 200 µL of FACS buffer, the cell pellet was resuspended in 200 µL of FACS buffer containing PI at a 1:1000 dilution for subsequent analysis.

### GenBank

The cDNA and amino acid sequences of the nanobodies have been deposited in GenBank under the following accession numbers:

- NN-224/TNFI-β: PV016701
- NN-223/TNFI-α: PV016702
- 05C08R3/TNFI-Nb1: PV016703
- 05B05R3/TNFI-Nb2: PV016704
- 03H04R3/TNFI-Nb3: PV016705.

### Statistical analysis

Data were analyzed using GraphPad Prism 0 software. IC50 values were determined using a nonlinear regression model ("log-(inhibitor) vs. response"). Differences between groups were assessed using one-way ANOVA followed by Tukey's post hoc test. A p-value of $< 0.05$ was considered statistically significant.

## Disclosure statement

Dr. Luciano D'Adamio is a Professor at Rutgers University and also the founder of NanoNewron, a biotechnology company focused on developing innovative therapeutics for central nervous system diseases. The contribution to this study of Pietro Sormanni, Aubin Ramon and Matthew Greenig was conducted in a consultancy capacity and was remunerated by NanoNewron LLC.

## Funding

The work was supported by the National Institute on Aging [R41AG080864, R01AG073182 and RF1AG064821].

## ORCID

Tao Yin http://orcid.org/0000-0003-0524-8075
Aubin Ramon http://orcid.org/0009-0002-5502-5961
Pietro Sormanni http://orcid.org/0000-0002-6228-2221
Luciano D'Adamio http://orcid.org/0000-0002-2204-9441

## References

1. Zouris G, Evangelopoulos DS, Benetos IS, Vlamis J. The use of TNF-α inhibitors in active ankylosing spondylitis treatment. Cureus. 2024;16:e61500. doi: 10.7759/cureus.61500.
2. Lopetuso LR, Cuomo C, Mignini I, Gasbarrini A, Papa A. Focus on anti-tumour necrosis factor (TNF)-α-related autoimmune diseases. IJMS. 2023;24(9):8187. doi: 10.3390/ijms24098187.
3. Leone GM, Mangano K, Petralia MC, Nicoletti F, Fagone P. Past, present and (foreseeable) future of biological anti-TNF alpha therapy. J Clin Med. 2023;12(4):1630. doi: 10.3390/jcm12041630.
4. Kawanishi M, Fujii Y. Pharmacological profiles and clinical efficacy of ozoralizumab (Nanozora((r)) 30 mg syringes for S.C. Injection), the first Nanobody((R)) compound in Japan. Nihon Yakurigaku Zasshi. 2023;158:490–499. doi: 10.1254/fpj.23051.
5. Crommelin HA, Vorselaars AD, van Moorsel CH, Korenromp IH, Deneer VH, Grutters JC. Anti-TNF therapeutics for the treatment of sarcoidosis. Immunotherapy. 2014;6(10):1127–1143. doi: 10.2217/imt.14.65.
6. Yu T, Zheng F, He W, Muyldermans S, Wen Y. Single domain antibody: development and application in biotechnology and biopharma. Immunological Rev. 2024;328(1):98–112. doi: 10.1111/imr.13381.
7. Hamers-Casterman C, Atarhouch T, Muyldermans S, Robinson G, Hamers C, Songa EB, Bendahman N, Hammers R. Naturally occurring antibodies devoid of light chains. Nature. 1993;363(6428):446–448. doi: 10.1038/363446a0.
8. Li T, Bourgeois JP, Celli S, Glacial F, Le Sourd AM, Mecheri S, Weksler B, Romero I, Couraud P-O, Rougeon F, et al. Cell-penetrating anti-GFAP VHH and corresponding fluorescent fusion protein VHH-GFP spontaneously cross the blood-brain barrier and specifically recognize astrocytes: application to brain imaging. Faseb J. 2012;26(10):3969–3979. doi: 10.1096/fj.11-201384.
9. Li T, Vandesquille M, Koukouli F, Dudeffant C, Youssef I, Lenormand P, Ganneau C, Maskos U, Czech C, Grueninger F, et al. Camelid single-domain antibodies: a versatile tool for in vivo imaging of extracellular and intracellular brain targets. J Control Release. 2016;243:1–10. doi: 10.1016/j.jconrel.2016.09.019.
10. Xiao G, Gan LS. Receptor-mediated endocytosis and brain delivery of therapeutic biologics int. The J Cell Biol. 2013;2013:703545. doi: 10.1155/2013/703545.
11. Sehlin D, Stocki P, Gustavsson T, Hultqvist G, Walsh FS, Rutkowski JL, Syvänen S. Brain delivery of biologics using a cross-species reactive transferrin receptor 1 VNAR shuttle. Faseb J. 2020;34(10):13272–13283. doi: 10.1096/fj.202000610RR.
12. Johnsen KB, Burkhart A, Thomsen LB, Andresen TL, Moos T. Targeting the transferrin receptor for brain drug delivery. Prog Neurobiol. 2019;181:101665. doi: 10.1016/j.pneurobio.2019.101665 .
13. Lee HJ, Engelhardt B, Lesley J, Bickel U, Pardridge WM. Targeting rat anti-mouse transferrin receptor monoclonal antibodies through blood-brain barrier in mouse. J Pharmacol Exp Ther. 2000;292(3):1048–1052. doi: 10.1016/S0022-3565(24)35388-1.
14. Hill JA, Wang D, Jevnikar AM, Cairns E, Bell DA. The relationship between predicted peptide–MHC class II affinity and T-cell activation in a HLA-DRβ1*0401 transgenic mouse model. Arthritis Res Ther. 2003;5(1):R40–48. doi: 10.1186/ar605.
15. Lazarski CA, Chaves FA, Jenks SA, Wu S, Richards KA, Weaver JM, Sant AJ. The kinetic stability of MHC class II: peptide complexes is a key parameter that dictates immunodominance. Immunity. 2005;23(1):29–40. doi: 10.1016/j.immuni.2005.05.009.
16. Kim A, Sadegh-Nasseri S. Determinants of immunodominance for CD4 T cells. Curr Opin Immunol. 2015;34:9–15. doi: 10.1016/j.coi.2014.12.005.
17. Wieczorek M, Abualrous ET, Sticht J, Alvaro-Benito M, Stolzenberg S, Noe F, Freund C. Major histocompatibility complex (MHC) class I and MHC class II proteins: conformational plasticity in antigen presentation. Front Immunol. 2017;8:292. doi: 10.3389/fimmu.2017.00292.
18. James EA, Moustakas AK, Bui J, Nouv R, Papadopoulos GK, Kwok WW. The binding of antigenic peptides to HLA-DR is influenced by interactions between pocket 6 and pocket 9. The J Immunol. 2009;183(5):3249–3258. doi: 10.4049/jimmunol.0802228.
19. Sant'angelo DB, Robinson E, Janeway CA Jr., Denzin LK. Recognition of core and flanking amino acids of MHC class II-bound peptides by the T cell receptor. Eur J Immunol. 2002;32:2510–2520. doi: 10.1002/1521-4141(200209)32:9<2510:AID-IMMU2510>3.0.CO;2-Q.
20. Aubin Ramon MA, Atkinson M, Saturnino A, Didi K, Visentin C, Ricagno S, Xu X, Greenig M, Sormanni P, Sormanni P. Assessing

antibody and nanobody nativeness for hit selection and humanization with AbNatiV. Nat Mach Intell. 2024;6(1):74–91. doi: 10.1038/s42256-023-00778-3.
21. Abanades B, Wong WK, Boyles F, Georges G, Bujotzek A, Deane CM. ImmuneBuilder: deep-learning models for predicting the structures of immune proteins. Commun Biol. 2023;6(1):575. doi: 10.1038/s42003-023-04927-7.
22. Rosace A, Bennett A, Oeller M, Mortensen MM, Sakhnini L, Lorenzen N, Poulsen, C., Sormanni, P. Automated optimisation of solubility and conformational stability of antibodies and proteins. Nature communications. 2023;14(1):1937. doi: 10.1038/s41467-023-37668-6.
23. Beirnaert E, Desmyter A, Spinelli S, Lauwereys M, Aarden L, Dreier T, Loris R, Silence K, Pollet C, Cambillau C, et al. Bivalent Llama single-Domain antibody fragments against tumor necrosis factor have picomolar potencies due to intramolecular interactions. Front Immunol. 2017;8:867. doi: 10.3389/fimmu.2017.00867.
24. Nakagomi D, Hanai S. Rapid improvement of rheumatoid arthritis symptoms with ozoralizumab: a case of progress monitored by musculoskeletal ultrasonography scand. J Rheumatol. 2025;54(3):217–218. doi: 10.1080/03009742.2025.2464451.
25. Mima M, Mishima-Tsumagari C, Nakano K, Morimoto M, Ogata H, Sakata M, Iwaoka R, Iwata K, Hachiuma K, Iwamoto K, et al. Structural design of the anti-TNFα therapeutic NANOBODY® compound, ozoralizumab, to support its potent and sustained clinical efficacy. Biochem Biophys Res Commun. 2024;734:150454. doi: 10.1016/j.bbrc.2024.150454.
26. Tracey D, Klareskog L, Sasso EH, Salfeld JG, Tak PP. Tumor necrosis factor antagonist mechanisms of action: a comprehensive review. Pharmacol Ther. 2008;117(2):244–279. doi: 10.1016/j.pharmthera.2007.10.001.
27. Cheng X, Shen Y, Li R. Targeting TNF: a therapeutic strategy for Alzheimer's disease. Drug Discov Today Today. 2014;19(11):1822–1827. doi: 10.1016/j.drudis.2014.06.029.
28. Boado RJ, Hui EK, Lu JZ, Zhou QH, Pardridge WM. Selective targeting of a TNFR decoy receptor pharmaceutical to the primate brain as a receptor-specific IgG fusion protein. J Biotechnol. 2010;146(1–2):84–91. doi: 10.1016/j.jbiotec.2010.01.011.
29. Butchart J, Brook L, Hopkins V, Teeling J, Puntener U, Culliford D, Sharples R, Sharif S, McFarlane B, Raybould R, et al. Etanercept in alzheimer disease: a randomized, placebo-controlled, double-blind, phase 2 trial. Neurology. 2015;84(21):2161–2168. doi: 10.1212/WNL.0000000000001617.
30. Tufan AN, Tufan F. Etanercept in alzheimer disease: a randomized, placebo-controlled, double-blind, phase 2 trial. Neurology. 2015;85(23):2083–2084. doi: 10.1212/01.wnl.0000475736.75775.25.
31. Plantone D, Pardini M, Righi D, Manco C, Colombo BM, De Stefano N. The role of TNF-α in Alzheimer's disease: a narrative review. Cells. 2023;13(1):54. doi: 10.3390/cells13010054.
32. Gonzalez Caldito N. Role of tumor necrosis factor-alpha in the central nervous system: a focus on autoimmune disorders. Front Immunol. 2023;14:1213448. doi: 10.3389/fimmu.2023.1213448.
33. Tarkowski E, Andreasen N, Tarkowski A, Blennow K. Intrathecal inflammation precedes development of Alzheimer's disease. J Neurol Neurosurg Psychiatry. 2003;74(9):1200–1205. doi: 10.1136/jnnp.74.9.1200.
34. Fillit H, Ding WH, Buee L, Kalman J, Altstiel L, Lawlor B, Wolf-Klein G. Elevated circulating tumor necrosis factor levels in Alzheimer's disease. Neurosci Lett. 1991;129(2):318–320 10.1016/0304-3940(91)90490-k. doi: 10.1016/0304-3940(91)90490-K.
35. Tarkowski E, Liljeroth AM, Minthon L, Tarkowski A, Wallin A, Blennow K. Cerebral pattern of pro- and anti-inflammatory cytokines in dementias. Brain Res Bull. 2003;61(3):255–260 10.1016/s0361-9230(03)00088-1. doi: 10.1016/S0361-9230(03)00088-1.
36. Tarkowski E, Tullberg M, Fredman P, Wikkelso C. Correlation between intrathecal sulfatide and TNF-α levels in patients with vascular dementia. Dement Geriatr Cogn Disord. 2003;15(4):207–211. doi: 10.1159/000068780.
37. Alvarez A, Cacabelos R, Sanpedro C, Garcia-Fantini M, Aleixandre M. Serum TNF-alpha levels are increased and correlate negatively with free IGF-I in alzheimer disease. Neurobiol Aging. 2007;28(4). doi: 10.1016/j.neurobiolaging.2006.02.012.
38. Perry RT, Collins JS, Harrell LE, Acton RT, Go RC. Investigation of association of 13 polymorphisms in eight genes in southeastern African American alzheimer disease patients as compared to age-matched controls. Am J Med Genet. 2001;105(4):332–342. doi: 10.1002/ajmg.1371.
39. Alawdi SH, El-Denshary ES, Safar MM, Eidi H, David MO, Abdel-Wahhab MA. Neuroprotective effect of nanodiamond in Alzheimer's disease rat model: a pivotal role for modulating NF-κB and STAT3 signaling. Mol Neurobiol. 2016;54(3):1906–1918. doi: 10.1007/s12035-016-9762-0.
40. Akiyama H, Barger S, Barnum S, Bradt B, Bauer J, Cole GM, Cooper, N.R., Eikelenboom, P., Emmerling, M., Fiebich, B.L., et al. Inflammation and Alzheimer's disease. Neurobiol Aging. 2000;21(3):383–421 10.1016/s0197-4580(00)00124-x. doi: 10.1016/S0197-4580(00)00124-X.
41. Guerreiro R, Wojtas A, Bras J, Carrasquillo M, Rogaeva E, Majounie E, Cruchaga C, Sassi C, Kauwe JSK, Younkin S, et al. TREM2 variants in Alzheimer's disease. N Engl J Med. 2013;368(2):117–127. doi: 10.1056/NEJMoa1211851.
42. Jonsson T, Stefansson H, Steinberg S, Jonsdottir I, Jonsson PV, Snaedal J, Bjornsson S, Huttenlocher J, Levey AI, Lah JJ, et al. Variant of TREM2 associated with the risk of Alzheimer's disease. N Engl J Med. 2013;368(2):107–116. doi: 10.1056/NEJMoa1211103 .
43. Watad A, McGonagle D, Anis S, Carmeli R, Cohen AD, Tsur AM, Ben-Shabat N, Luigi Bragazzi N, Lidar M, Amital H, et al. TNF inhibitors have a protective role in the risk of dementia in patients with ankylosing spondylitis: results from a nationwide study pharmacol res. Pharmacol Res. 2022;182:106325. doi: 10.1016/j.phrs.2022.106325.
44. Chou RC, Kane M, Ghimire S, Gautam S, Gui J. Treatment for rheumatoid arthritis and risk of Alzheimer's disease: a nested case-control analysis CNS drugs. CNS Drugs. 2016;30(11):1111–1120 10.1007/s40263-016-0374-z. doi: 10.1007/s40263-016-0374-z.
45. Tobinick E, Gross H, Weinberger A, Cohen H. TNF-alpha modulation for treatment of Alzheimer's disease: a 6-month pilot study. Med Gen Med. 2006;8:25. https://www.ncbi.nlm.nih.gov/pubmed/16926764.
46. Shi JQ, Wang BR, Jiang WW, Chen J, Zhu YW, Zhong LL, Zhang Y-D, Xu J. Cognitive improvement with intrathecal administration of infliximab in a woman with Alzheimer's disease. J Am Geriatr Soc. 2011;59(6):1142–1144. doi: 10.1111/j.1532-5415.2011.03445.x.
47. Hickman SE, Allison EK, El Khoury J. Microglial dysfunction and defective β-amyloid clearance pathways in aging Alzheimer's disease mice. J Neurosci. 2008;28(33):8354–8360. doi: 10.1523/JNEUROSCI.0616-08.2008.
48. He P, Zhong Z, Lindholm K, Berning L, Lee W, Lemere C, Staufenbiel M, Li R, Shen Y. Deletion of tumor necrosis factor death receptor inhibits amyloid β generation and prevents learning and memory deficits in Alzheimer's mice. J Cel Biol. 2007;178(5):829–841. doi: 10.1083/jcb.200705042.
49. Beattie EC, Stellwagen D, Morishita W, Bresnahan JC, Ha BK, Von Zastrow M, Beattie MS, Malenka RC. Control of synaptic strength by glial TNFα. Science. 2002;295(5563):2282–2285. doi: 10.1126/science.1067859.
50. Stellwagen D, Beattie EC, Seo JY, Malenka RC. Differential regulation of AMPA receptor and GABA receptor trafficking by tumor necrosis factor-α. J Neurosci. 2005;25(12):3219–3228. doi: 10.1523/JNEUROSCI.4486-04.2005.
51. Stellwagen D, Malenka RC. Synaptic scaling mediated by glial TNF-α. Nature. 2006;440(7087):1054–1059. doi: 10.1038/nature04671.
52. Cirrito JR, Kang JE, Lee J, Stewart FR, Verges DK, Silverio LM, Bu G, Mennerick S, Holtzman DM. Endocytosis is required for synaptic activity-dependent release of amyloid-β in vivo. Neuron.

2008;58(1):42–51 S0896–6273(08)00124–4 [pii]10.1016/j.neuron.2008.02.003.
53. Cirrito JR, Yamada KA, Finn MB, Sloviter RS, Bales KR, May PC, Schoepp DD, Paul SM, Mennerick S, Holtzman DM. Synaptic activity regulates interstitial fluid amyloid-β levels in vivo. Neuron. 2005;48(6):913–922. doi: 10.1016/j.neuron.2005.10.028.
54. Wu JW, Hussaini SA, Bastille IM, Rodriguez GA, Mrejeru A, Rilett K, Sanders DW, Cook C, Fu H, Boonen RACM, et al. Neuronal activity enhances tau propagation and tau pathology in vivo. Nat Neurosci. 2016;19(8):1085–1092. doi: 10.1038/nn.4328.
55. Ren S, Breuillaud L, Yao W, Yin T, Norris KA, Zehntner SP, D'Adamio L. TNF-α–mediated reduction in inhibitory neurotransmission precedes sporadic Alzheimer's disease pathology in young Trem2 rats. J Biol Chem. 2021;296:100089. doi: 10.1074/jbc.RA120.016395.
56. Tambini MD, D'adamio L. Trem2 splicing and expression are preserved in a human Aβ-producing, rat knock-in model of Trem2-R47H Alzheimer's risk variant. Sci Rep. 2020;10(1):4122. doi: 10.1038/s41598-020-60800-1.
57. Ren S, Yao W, Tambini MD, Yin T, Norris KA, D'adamio L. Microglia TREM2(R47H) alzheimer-linked variant enhances excitatory transmission and reduces LTP via increased TNF-alpha levels. Elife. 2020;9. doi: 10.7554/eLife.57513.